Journal of Medicinal Chemistry

pubs.acs.org/jmc

Drug Annotation

Design, Synthesis, and Pharmacological Characterization of a Neutral, Non-Prodrug Thrombin Inhibitor with Good Oral Pharmacokinetics

Alexander Hillisch,* Kersten M. Gericke, Swen Allerheiligen, Susanne Roehrig, Martina Schaefer, Adrian Tersteegen, Simone Schulz, Philip Lienau, Mark Gnoth, Vera Puetter, Roman C. Hillig, and Stefan Heitmeier

Cite This: https://dx.doi.org/10.1021/acs.jmedchem.0c01035

Read Online

ACCESS | Metrics & More | Article Recommendations | Supporting Information

ABSTRACT: Despite extensive research on small molecule thrombin inhibitors for oral application in the past decades, only a single double prodrug with very modest oral bioavailability has reached human therapy as a marketed drug. We have undertaken major efforts to identify neutral, non-prodrug inhibitors. Using a holistic analysis of all available internal data, we were able to build computational models and apply these for the selection of a lead series with the highest possibility of achieving oral bioavailability. In our design, we relied on protein structure knowledge to address potency and identified a small window of favorable physicochemical properties to balance absorption and metabolic stability. Protein structure information on the pregnane X receptor helped in overcoming a persistent cytochrome P450 3A4 induction problem. The selected compound series was optimized to a highly potent, neutral, non-prodrug thrombin inhibitor by designing, synthesizing, and testing derivatives. The resulting optimized compound, BAY1217224, has reached first clinical trials, which have confirmed the desired pharmacokinetic properties.

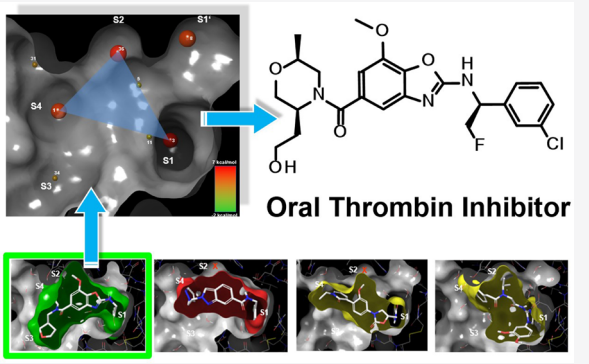

INTRODUCTION

Thrombin (or blood coagulation factor IIa) can be regarded as the key target in the blood coagulation cascade. The chase for oral thrombin inhibitors thus began in the late 1970s, leading to ximelagatran,[1] and have culminated in only one marketed product, dabigatran etexilate[2] (Figure 1), a benzamidine double prodrug with only very modest oral bioavailability. In the late 1990s alternative targets, such as FXa, were explored with the discovery that the highly basic, cell permeation-preventing benzamidine group can be replaced by a neutral chloro or methoxyaryl group.[3] Both aspects led to the fact that thrombin drug discovery was overtaken by FXa research, producing compounds with clearly superior pharmacokinetics. Those compounds (rivaroxaban,[4] apixaban,[5] edoxaban,[6] betrixaban[7]) finally entered the market and are highly successful remedies. Results from FXa research were transferred back to thrombin with some success. Merck and AstraZeneca have reported on neutral thrombin inhibitors.[8−10]The neutral prodrug AZD8165 entered clinical trials but showed short half-life in healthy male volunteers. To the best of our knowledge, currently there is no neutral thrombin inhibitor in clinical development.

In this paper, we analyze the molecular features that lead to a significantly lower oral druggability of thrombin in comparison to FXa and describe the drug discovery efforts at Bayer AG to identify neutral, orally available thrombin inhibitors.

RESULTS AND DISCUSSION

Druggability of Thrombin. The Bayer AG search for novel thrombin inhibitors started with a high-throughput screening campaign of our in-house compound pool. The approach was complemented with protein structure-based design. These efforts resulted in four distinct chemical series. During lead optimization phases, several thousand compounds were synthesized and characterized.[11−16] However, we had to face up to the significantly lower druggability of thrombin in comparison to FXa.

Received: June 17, 2020

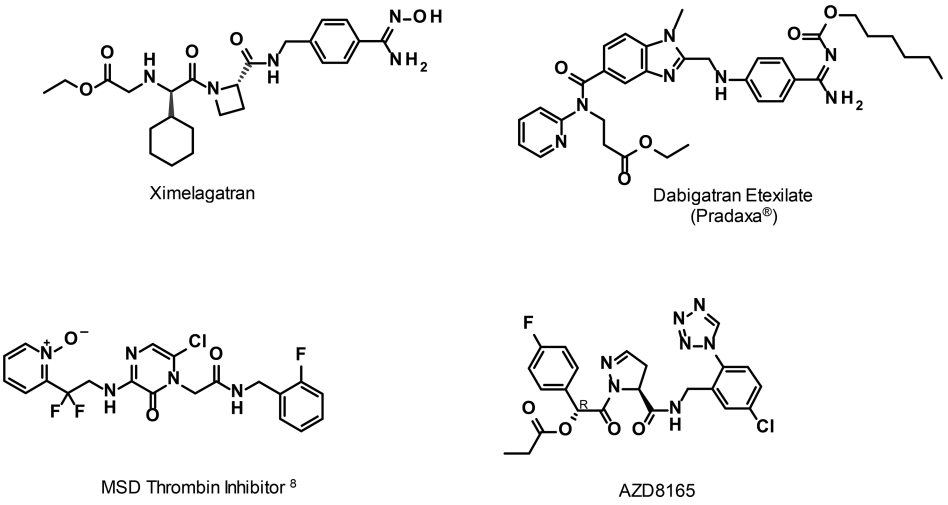

Figure 1. Selected small molecule, oral thrombin inhibitors.

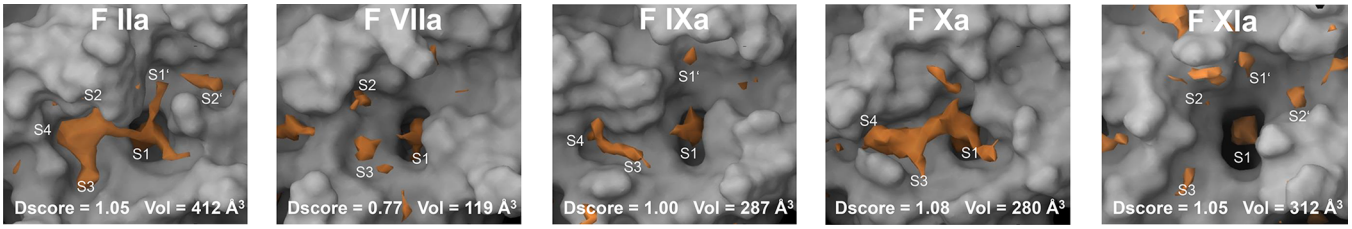

Figure 2. SiteMap analysis of selected serine proteases from the blood coagulation cascade.

The druggability of thrombin has been analyzed in detail and classified as being "difficult".[17] Upon analysis of the X-ray structures of selected serine proteases from the blood coagulation cascade using the SiteMap[18] approach, it becomes evident that FXa has the binding site with the highest oral druggability (Dscore 1.08, volume 280 Å^3), followed by thrombin (Dscore 1.05, volume 412 Å^3) and FXIa (Dscore 1.05, volume 312 Å^3, Table S1). Both thrombin and FXa stand out from other proteases of the coagulation cascade due to their higher hydrophobicity (Figure 2, orange volume). The main difference between thrombin and FXa is the significantly larger size of the thrombin pocket which is attributed to the deep S2 pocket. The S1 pockets are nearly identical for the three top-ranked proteases, whereas FVIIa and FIXa both differ in one amino acid from the other three proteases: Ala190 is substituted by a serine, forming a hydrogen bond with a deeply buried water molecule and preventing its displacement by P1 chloroaryl-containing inhibitors. The substrate binding sites of the latter two proteases can be regarded as orally undruggable (Table S1, Supporting Information).

Lead Finding and Lead Series Selection. In 2009, we initiated a novel attempt aimed at the difficult, but presumably resolvable, task of identifying non-prodrug, orally bioavailable inhibitors of thrombin.

First, we wanted to identify a window of physicochemical properties that would lead to favorable *in vitro* and subsequently *in vivo* pharmacokinetics. The average clogP,[19] topological polar surface area (tPSA),[20] and corrected molecular weight (MW_{corr})[21] for 521 exemplified compounds in our patents[11−16] is 5.1, 84 Å^2, and 488 Da, respectively. This nicely reflects the properties of the large, hydrophobic thrombin substrate binding pocket. The properties of one compound of this pool stood out, capturing our attention (Figure 3).

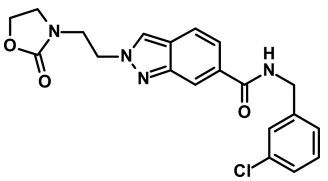

Figure 3. Structure of compound **1** as weak thrombin inhibitor with interesting physicochemical properties.

Compound **1** has convincing metabolic clearance (*in vivo* iv blood clearance, rat, 1.4 L h^{-1} kg^{-1}) and cell permeability (*in vitro* Caco-2 P_{app}(A−B) cell permeation, 62 nm/s). Unfortunately, this compound is only a relatively weak thrombin inhibitor (IC_{50} = 220 nM). With a clogP of 3.2 and a PSA of 76 Å^2, **1** served as a prototype with respect to physicochemical properties. From the analysis of all our patented examples, we speculated that those with a significantly reduced lipophilicity (clogP = 2.5−3.5) and a PSA not larger than approximately 105 Å^2 would result in compounds with a higher chance of oral bioavailability.

The task was then to find the right structural inhibitor series that would allow subnanomolar thrombin inhibition within the frame of physicochemical constraints.

To do so, we analyzed the substrate binding pocket of thrombin with WaterMap,[22,23] a molecular dynamics approach that characterizes solvent structure and energetics within a ligand binding pocket of a target protein. By use of inhomogeneous solvation theory,[24] the system interaction energy and excess entropy for each water molecule in the

https://dx.doi.org/10.1021/acs.jmedchem.0c01035
J. Med. Chem. XXXX, XXX, XXX−XXX

substrate binding pocket are calculated. In principle, the less energetically (enthalpically and/or entropically) favorable expelled waters are, the more favorable is their contribution to the binding free energy. In Figure 4, hydration sites with the

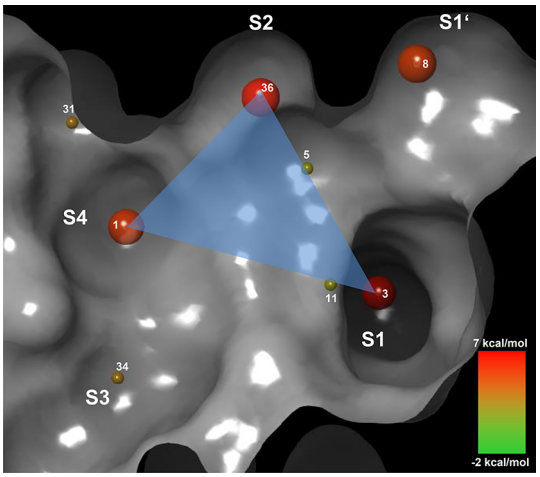

Figure 4. WaterMap hydration sites in the substrate binding pocket of thrombin. Sites are color- and size-coded with regard to the modeled hydration free energy (high ΔG large, reddish; low ΔG small, greenish).

color-coded modeled highest free energy (ΔG) are displayed (for detailed values, see Table S2, Supporting Information). The analysis suggested that the top three hydration sites (site 3, ΔG = 6.9 kcal/mol; site 36, ΔG = 6.6 kcal/mol; site 1, ΔG = 5.6 kcal/mol) with the highest free energy gain upon complex formation are the ones located in the S1, S2, and S4 pockets of thrombin. Hydration site 8 (ΔG = 5.5 kcal/mol) was not further considered since it lies somewhat outside the space ligands typically occupy. Two less important hydration sites (5 and 11) lie on the edges of a hypothetical triangle that connects the S1, S2, and S4 pockets. An interesting hydration site, site 31, was identified on the border of the S4 pocket (ΔG = 3.5 kcal/mol), along with a site within the S3 pocket (site 34, ΔG = 3.4 kcal/mol).

As a result of these calculations, we hypothesized that the ideal thrombin inhibitor would occupy only the S1, S2, and S4 pockets; to keep lipophilicity, PSA, and molecular weight low, it would not extend with larger substituents into other hydrophobic subpockets. Following that theory, we cocrystallized representative compounds from all four chemical series with thrombin and analyzed their binding features in light of the "three-pocket hypothesis".

The physicochemical properties and some SAR features of the four series (Figure 5) can be explained as follows (for detailed physicochemical values, see Table S3, Supporting Information):

Indazoles. Branching from a central indazole core, this series occupies the S1 pocket with a chloroaryl residue and the S4 pocket with an aromatic or cycloaliphatic residue. Due to the geometry of the indazole, the S2 pocket can only be addressed by a "one-heavy-atom" substituent at position 4. But with that substituent, the S2 pocket is not completely filled. Substitution with chlorine (**3**) diminishes inhibition slightly from an IC_{50} of 173 nM (for 4-unsubstituted **2**) to 225 nM, whereas a "two-heavy-atom" methoxy substitution (**4**) leads to a loss of activity by a factor of 3 (IC_{50} = 464 nM) (Figure 5) as the aromatic CH at position 3 of the indazole pushes the methoxy carbon toward the 5-position. This conformation is energetically favored by 2.8 kcal/mol (OPLS2005 force field)[25] but does not fit into the S2 pocket (Figure 6). The overall properties are that this class is relatively lipophilic (av. clogP = 4.6) with a small PSA of 68 Å^2 (Table S3, Supporting Information).

Oxazolidinones. The main pharmacophoric residues are a chlorothiophene as P1 and a five- or six-membered heterocycle or heteroaryl, as P4 residue (e.g., **5**). The central phenyl residue allows addressing of the S2 pocket. However, complete filling of this pocket requires a long, flexible, at least "three-

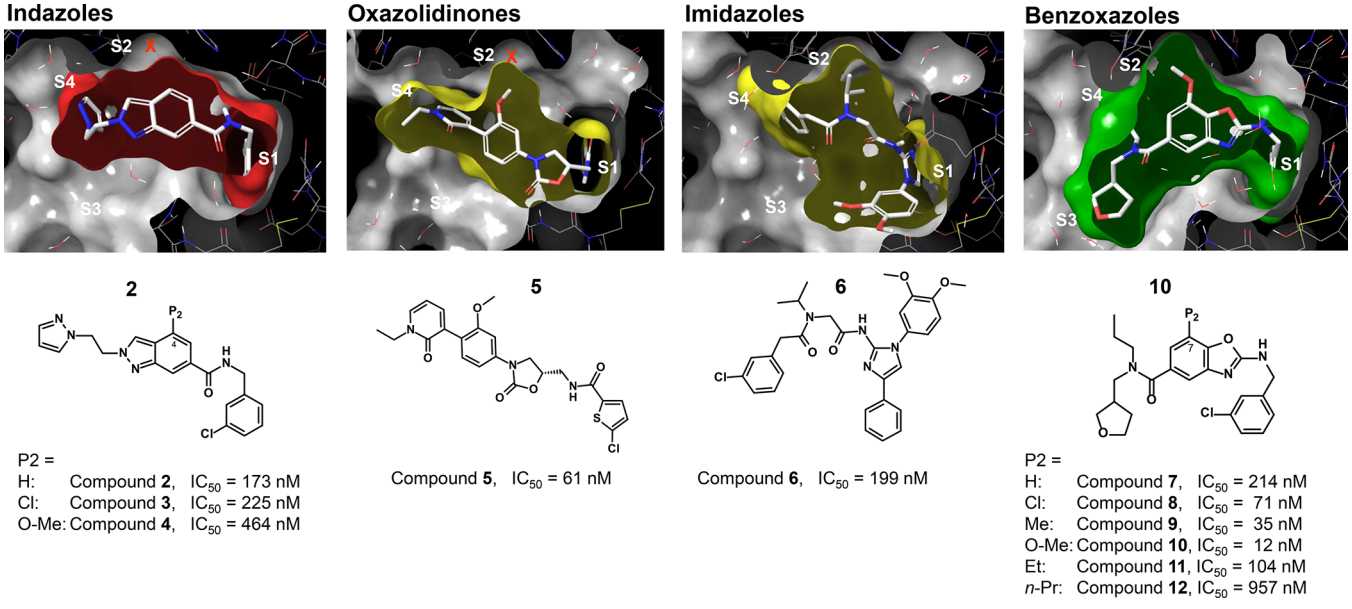

Figure 5. X-ray structures of potential lead compounds in complex with thrombin. All four lead series were discovered by internal HTS at Bayer. The red x highlights unoccupied volume in the S2 pocket. Compound surface colors represent suitability of lead structure to archive highly potent orally bioavailable thrombin inhibitors (red, low; yellow, medium; green, high) and show the degree of filling of the S2 pocket.

https://dx.doi.org/10.1021/acs.jmedchem.0c01035
J. Med. Chem. XXXX, XXX, XXX−XXX

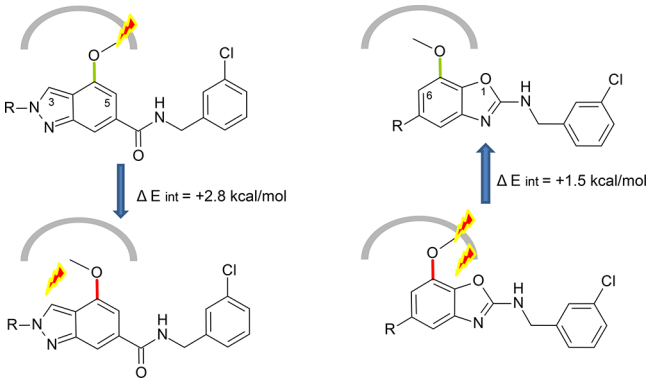

Figure 6. Comparison of indazole vs benzoxazole fit in the S2 pocket (gray).The blue arrow shows the difference in internal energy between two conceivable conformations each.

heavy-atom" group. A rigid methoxy substituent (**5**) does not completely fill the S2 pocket (Figure 5). P2 residues usually improve selectivity toward FXa inhibition. In contrast to the other three series, oxazolidinones bind less deeply in the substrate pocket. They occupy volume around the more exposed ester binding pocket (EBP) and the S3 pocket and do not directly contact His57 and Ser195. The average physicochemical properties, namely, low clogP (3.2), medium PSA, and a lipophilic ligand efficiency[26] (LLE) of 4.0, of the oxazolidinones are attractive, being superior to the other three series.

Imidazoles. The imidazole core is substituted with two aromatic moieties occupying the S1 pocket and the EBP, a subpocket on the rim of the S1 pocket directly above the disulfide bond formed by Cys191 and Cys220. An aliphatic branched residue fills the S2 pocket; the S4 pocket is occupied by different bulky substituents (**6**). Filling of the EBP is essential for activity. The resulting high mass (av 521 Da) and lipophilicity (av clogP = 5.6) contribute to the low average ligand efficiency[27] (LE = 0.26) and LLE (1.7) which are the worst within these four series.

Table 1. Initial SAR of Rigid P4 Residues[a]

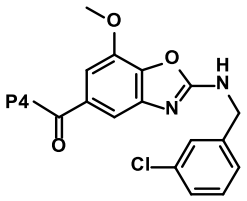

Compd	P4	Stereo-chemistry	Thrombin IC_{50} [nM]	Caco-2 flux P_{app} (A–B) [nm/s]	CL_b (hepatocytes) [L/h/kg]	PXR MEC [μM]	clogP	MW_{corr}	PSA [Å^2]	LE (with MW_{corr})	LLE (with clogP)
10	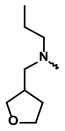	racemate	12	246	3.9	n.d.	4.0	442	77	0.34	3.9
13		single isomer	180	n.d.	n.d.	n.d.	3.8	370	68	0.34	3.0
14		single isomer	47	n.d.	3.5	n.d.	4.8	398	68	0.35	2.5
15		single isomer	40	n.d.	n.d.	n.d.	4.8	398	68	0.35	2.6
16		single isomer	441	n.d.	n.d.	n.d.	3.3	386	77	0.31	3.0
17		single isomer	27	n.d.	n.d.	1.3	4.4	414	77	0.35	3.2
18	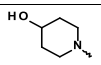	single isomer	352	71	1.3	3.1	2.3	400	88	0.31	4.2
19	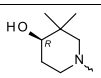	single isomer	35	n.d.	3.1	6.3	3.3	428	88	0.33	4.2
20a	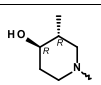	single isomer	10	126	2.3	0.69	2.8	414	88	0.37	5.2
20b	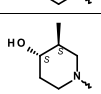	single isomer	120	n.d.	2.2	n.d.	2.8	414	88	0.32	4.1

[a]n.d.: not determined.

https://dx.doi.org/10.1021/acs.jmedchem.0c01035
J. Med. Chem. XXXX, XXX, XXX−XXX

Benzoxazoles. Branching from a central benzoxazole core, this series occupies the S1 pocket with a chloroaryl residue and the S4 pocket with different substituents. In contrast to the indazoles, the S2 pocket can be filled perfectly with a "two-heavy-atom" residue like methoxy. This substituent seems to be the local optimum (Figure 5). The oxygen at position 1 of benzoxazole pushes the methoxy carbon toward the 6-position. This conformation is energetically favored by 1.5 kcal/mol and fits exactly into the S2 pocket (Figure 6). Derivatives lacking substitution at position 7 (**7**) or with a "one-heavy-atom" substituent (**8** and **9**) are significantly less potent. Interestingly, an ethyl residue prefers conformations in which the terminal carbon is positioned above or below the aromatic plane; **11** thus loses activity by a factor of nearly 10 in comparison to the methoxy derivative **10**. *N*-Propyl substitution (**12**) leads to a loss of inhibitory activity by a factor of 80 relative to **10**. The average properties of this series (high lipophilicity, clogP = 5.1; low LLE, 1.7) are unfavorable.

Despite the poor physicochemical properties of the benzoxazole compound class, it was selected as the most promising of the four classes. Our decision was based on the perfect fit of the methoxy-substituted core to the S2 pocket, in conjunction with a mass efficient addressing of the S1 pocket by a chlorobenzyl residue and a binding mode that buries the compound deep inside the substrate pocket. We planned to occupy the S4 pocket with rigid substituents, which should result in high-affinity compounds, and to decorate future compounds with more polar binding substituents, to reduce the overall lipophilicity and stay within the window of physicochemical properties, presumably leading to good oral pharmacokinetics. Other series with apparently more attractive physicochemical properties of, at that time, existing compounds (e.g., oxazolidinones) were deprioritized in favor of benzoxazoles which showed a more attractive binding mode and facilitated planning of virtual compounds in terms of their physicochemical properties.

Initial Lead Optimization. Lead optimization started with the branched P4 benzoxazole **10** (Table 1). This compound is characterized by flexible side chains as P3/P4 residues and a high lipophilicity. To gain potency and introduce more polarity, we substituted the flexible P4 residue by heterocycles. An unsubstituted pyrrolidine resulted in an only moderately active **13**. Docking studies suggested substitution at the 2- and/or 3-position of the pyrrolidine to replace water molecules buried in the S3 and S4 pockets (Figure 4). Dimethyl substitution at either position (**14** and **15**) significantly increased potency and lipophilicity. To introduce polarity, further reduce flexibility, and make use of more appropriate exit vectors for substituents that enable displacement of energetically unfavorable water molecules (Figure 7), we changed to morpholine. The unsubstituted morpholine derivative **16** displayed only weak activity. Since we intended to fill the S4 pocket completely, 3,3-dimethyl substitution was introduced (**17**) which increased inhibition to an IC_{50} of 27 nM. This design hypothesis was verified with an X-ray cocrystal structure of **17** with thrombin (see Table S4, Supporting Information). To install polarity, the S4 pocket was analyzed with regard to exposed hydrogen-bond acceptor functionalities. The closest carbonyl backbone group is Glu97A. Considering that the backbone NH of Glu97A is not hydrogen-bonded intramolecularly within thrombin, we expected some flexibility of the amide group and hoped to be able to form a hydrogen bond with a hydroxyl group at position 4 of an aliphatic six-membered ring. The resulting 4-hydroxypiperidine derivative **18** was only modestly active. However, clogP was significantly reduced to 2.3 and rat *in vitro* hepatocyte clearance was improved (1.3 L h^{-1} kg^{-1}). Hoping to increase thrombin inhibition, the piperidine was substituted at position 3 with a geminal dimethyl group (**19**) or a methyl group (**20a**), displacing a buried water molecule in the S4 pocket. **20a**, having a low molecular weight (MW = 414 Da) and balanced polarity (PSA = 88 $Å^2$, clogP = 2.8), was a significant step forward toward orally active thrombin inhibitors, and it was broadly characterized.

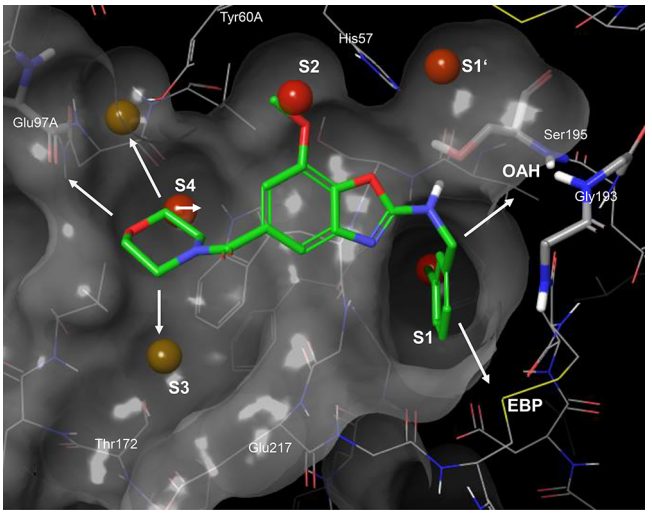

Figure 7. Modeled complex of **16** in thrombin (based on the X-ray structure of **10** in complex with thrombin). S1, S2, and S4 pockets, the oxyanion hole (OAH), and the ester binding pocket (EBP) are displayed.

Characterization of 20a. **20a** showed strong thrombin inhibition (biochemical IC_{50} = 10 nM; in human plasma, IC_{50} = 60 nM) and a doubling of clotting time (prothrombin time, PT) at 6 μM (EC_{200}). It had excellent permeation properties [P_{app}(A−B) = 126 nm/s, Caco-2 assay] and a moderate *in vitro* hepatocyte clearance (2.3 L h^{-1} kg^{-1}). In an *in vivo* rat pharmacokinetic study, blood clearance, $t_{1/2}$, and oral bioavailability were found to be moderate (1.7 L h^{-1} kg^{-1}, 1.3 h, and 46%, respectively; see Table 5). **20a** did not show any CYP inhibition, up to the highest concentration tested (20 μM), of the major enzymes, but a strong CYP3A4 induction effect via the pregnane X receptor (PXR) pathway was discovered. The onset of CYP3A4 induction in human hepatocytes was above 370 ng/mL (Table 5), and trans-activation of human PXR started at a minimum efficacious concentration (MEC) of 0.69 μM (~300 ng/mL) and was regarded as major optimization parameter.

To overcome PXR binding and thus CYP3A4 induction, we carried out cocrystallization experiments with the PXR ligand binding domain and several compounds, among them **17** and **20a**; however, cocrystallization was successful only for **17**. Although the weak density indicated occupancy of only 0.70, the chlorophenyl residue and the dimethylmorpholine group could be positioned unambiguously (Figure 8). The compound binds to the PXR with the chlorophenyl moiety pinched between Trp299 and Phe288 and forming a stacking interaction with Trp299. The chlorine is in close contact with Val211 and Leu209. The benzoxazole nitrogen serves as a hydrogen-bond acceptor interacting with the Gln285 side

https://dx.doi.org/10.1021/acs.jmedchem.0c01035
J. Med. Chem. XXXX, XXX, XXX−XXX

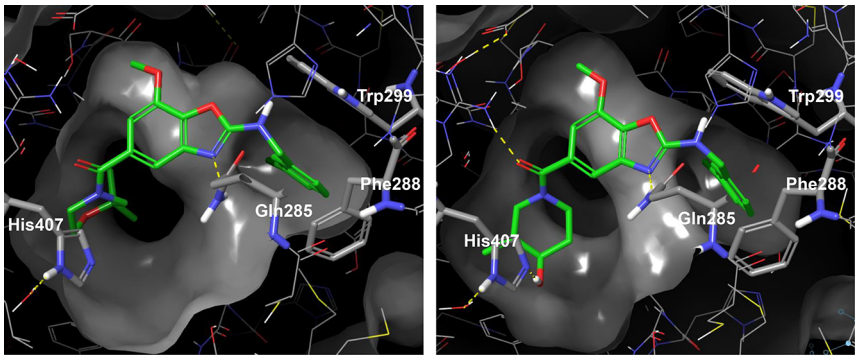

Figure 8. X-ray structure of **17** bound to the PXR ligand binding domain (left, PDB code 6TFI) and induced fit docking pose of **20a** in the PXR (right).

chain. The dimethylmorpholine occupies a hydrophobic pocket formed by Leu206, Leu240, and Ile414. Nevertheless, this X-ray structure did not explain the strong PXR binding of **20a**. Assuming a similar binding mode on the PXR for the dimethylmorpholine and 4-hydroxypiperidine P4 residues, the latter would position a polar hydroxyl group right between three hydrophobic amino acid side chains. Since this was regarded unlikely, an induced fit docking with Glide SP[28] on the PXR:**17** complex was performed. His407, Arg410, and Gln285 were treated flexibly. As result, the docking suggested a different orientation of the piperidine in comparison to the morpholine moiety (Figure 8). While the piperidinyl methyl group occupies a subpocket formed by Leu410 and Ile414, the 4-hydroxyl group forms a strong hydrogen bond with His407, explaining the CYP induction properties with a somewhat different binding mode than that observed for **17**. This binding hypothesis is further supported by the analysis of **19** in the PXR assay showing a significant reduction in PXR transactivation (MEC = 6.3 μM, 9-fold relative to **20a**; Table 1). The additional methyl group is thought to shield the hydroxyl group and thus would prevent hydrogen-bond formation with His407. The specific binding mode of **20a** with the PXR was not observed for **19** when the same induced fit docking protocol was applied.

Lead Optimization. The initial plans for further lead optimization could then be summarized as follows.

(i) Attempt to increase thrombin inhibition with conformationally restrained P4 residues displacing or replacing two water molecules in the S4 pocket and optionally also in the S3 pocket.

(ii) Attempt to decrease PXR binding to reduce CYP3A4 induction by modulating hydrogen-bond acceptor strength of the benzoxazole nitrogen to diminish contact with Gln285 and/or by introducing polarity in P1 to reduce binding in the hydrophobic cleft between Trp299 and Phe288.

(iii) Attempt to maintain the balance between absorption and metabolic clearance. Since **20a** already displayed a good balance of main pharmacokinetic optimization parameters, derivatives with physicochemical properties similar to **20a** and within the originally defined window (clogP = 2.5−3.5, PSA < 105 Å^2) would be synthesized. Analysis of several hundred derivatives indicated that P4 residues containing one hydroxyl group, one hydrogen-bond acceptor, and a few (2−4) additional carbon atoms would lead to the desired properties. In addition, we intended to block the P1 benzyl position with small substituents to decrease metabolic attack.

Exploring the SAR of P1 and the Bicyclic Core. To evaluate the planned modifications of P1, we kept P4 constant with substituent 3-methyl-4-hydroxypiperidine. Compounds in Table 2 are racemic mixtures of two isomers with either *cis* or *trans* configuration of the piperidine substituents. In comparison to the single most active isomer **20a**, the racemate **20rac** loses a factor of ∼2.5 in thrombin inhibition, while *in vitro* pharmacokinetic parameters were very similar.

To introduce some polarity in P1, *m*-chlorobenzyl was replaced by the four possible chloropyridine analogues keeping the chlorine position constant. As expected, 4-chloro-2-pyridyl (**21**) was the most potent derivative but, nevertheless, loses a factor of ∼9 in thrombin inhibition compared to **20rac**. Of the four P1 chloropyridine isomers, **21** is the only isomer leading to solvent exposure of the pyridine nitrogen when bound to thrombin. The other three isomers were significantly weaker with respect to thrombin inhibition. Thrombin lacks any hydrogen-bond donor functionalities in the S1 pocket. The pyridine nitrogen in **22** and **23** is close to polar groups (Asp189 and Gly219 backbone carbonyl, respectively) leading to electrostatic repulsion and consequently inactivity. In **24**, the pyridine nitrogen is placed in a lipophilic environment resulting in a moderate loss of activity compared to **20rac**. The position para to the chlorine residue in *m*-chlorobenzyl was further explored with fluorine and hydroxyl substituents. The P1 hydroxyl proton of **26** was expected to form a hydrogen bond with the backbone carbonyl of Gly219, similar to the bioisosteric 5-chloroindole of FXa inhibitors.[29] The additional hydroxyl and fluorine group led to a moderate decrease in thrombin affinity. To reduce potential metabolic attack at the benzylic P1 position, methyl, trifluoromethyl, cyclopropyl, and cyclobutyl were introduced. The *R*-configured P1 residue **27b** with a methyl substituent only lost a factor of 2 with regard to thrombin inhibition (vs **20rac**). To vary hydrogen-bond acceptor strength at both polar atoms of the core and to reduce the hydrogen-bond strength to Gln285 in the PXR (Figure 8), derivatives such as the inverted benzoxazole **31** and triazolopyridine **32** were synthesized. Interestingly and unexpectedly, the inverted benzoxazole was nearly inactive while the triazolopyridine lost a factor of ∼24 in thrombin inhibition. Quantum mechanical calculations at the OPBE/cc-pvtz level retrospectively could explain the significantly reduced hydrogen bond acceptor strengths of the inverted benzoxazole oxygen. In addition, the benzoxazole nitrogen is a polar strong H-bond acceptor but not involved in hydrogen bonding with thrombin which in addition most likely contributes to the significantly reduced binding affinity.

https://dx.doi.org/10.1021/acs.jmedchem.0c01035
J. Med. Chem. XXXX, XXX, XXX−XXX

Table 2. P1 and Core Modifications to Address PXR Binding[a]

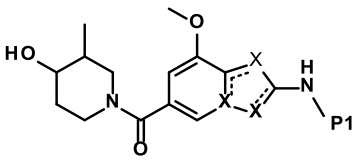

Compd	Core	P1	Stereochemistry	Thrombin IC_{50} [nM]	Caco-2 flux P_{app} (A–B) [nm/s]	CL_h (hepatocytes) [L/h/kg]	PXR MEC [μM]	clogP	MW_{corr}	PSA [Å^2]	LE (with MW_{corr})	LLE (with clogP)
20rac			racemate, *trans*	25	84	2.7	1.4	2.8	414	88	0.35	4.9
21			racemate, *trans*	190	41	0.86	3.6	1.4	415	101	0.31	5.4
22			racemate, *trans*	7200	9.3	2.4	n.d.	1.4	415	101	0.23	3.8
23			racemate, *trans*	6900	n.d.	n.d.	n.d.	1.4	415	101	0.24	3.8
24			racemate, *trans*	580	n.d.	n.d.	n.d.	1.4	415	101	0.28	4.9
25		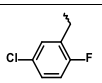	racemate, *trans*	300	n.d.	n.d.	n.d.	2.9	418	88	0.29	3.6
26		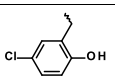	4 isomers (rac. *cis* and *trans* mixture)	170	n.d.	n.d.	8.3	2.4	430	108	0.30	4.4
27a		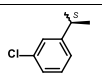	2 diastereomers, *trans*	5100	n.d.	n.d.	n.d.	3.1	428	88	0.23	2.2
27b		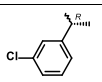	2 diastereomers, *trans*	48	n.d.	n.d.	n.d.	3.1	428	88	0.32	4.2
28		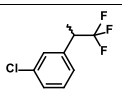	8 isomers (mixture of all possible stereoisomers)	790	n.d.	n.d.	n.d.	3.6	440	88	0.25	2.5
29		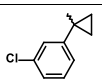	racemate, *cis*	120	n.d.	2.8	n.d.	3.1	440	88	0.30	3.8
30		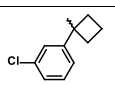	4 isomers (rac. *cis* and *trans* mixture)	8200	n.d.	n.d.	n.d.	3.7	454	88	0.21	1.4
31			racemate, *trans*	3900	n.d.	n.d.	n.d.	2.8	414	88	0.25	2.6
32			racemate, *trans*	470	71	2.1	20	1.8	414	92	0.29	4.6

[a]n.d.: not determined.

In summary, the P1 and core SAR study identified several modifications that offered a path forward to solve the PXR-mediated CYP3A4 induction issue and increase metabolic stability. Selected derivatives, designed with insight from X-ray structural analysis, corroborated our PXR binding mode and reduced PXR transactivation. Of special interest in that regard was the introduction of the 4-chloro-2-pyridyl residue (**21**, PXR MEC = 3.6 μM) as polar spot in a hydrophobic cleft of

https://dx.doi.org/10.1021/acs.jmedchem.0c01035
J. Med. Chem. XXXX, XXX, XXX−XXX

Table 3. Exploring P4 with Piperidine and Morpholine for Potent Substituents in Defined Physicochemical Space[a]

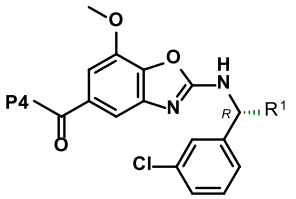

Compd	P4	R^1	Stereochemistry	Thromb in IC_{50} [nM]	Caco-2 flux P_{app} (A–B) [nm/s]	CL_h (hepatocytes) [L/h/kg]	PXR MEC [μM]	clogP	MW_{corr}	PSA [Å^2]	LE (with MW_{corr})	LLE (with clogP)
33a		H	6 isomers	66	127	3.4	n.d.	3.3	428	88	0.30	3.6
33b		H	single isomer [b]	45	n.d.	n.d.	2.6	3.3	428	88	0.32	4.0
34		H	2 diastereomers	13	n.d.	3.7	n.d.	3.8	442	88	0.34	4.1
35		H	4 isomers	8	138	3.8	0.26	3.7	454	88	0.34	4.4
36	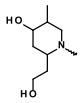	H	2 diastereomers	0.27	9.4	0.27	0.81	2.5	458	108	0.40	7.1
37a	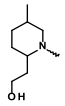	H	2 diastereomers, *cis*	4.3	191	3.8	0.32	4.6	442	88	0.36	3.8
37b	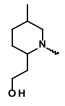	H	single isomer[b]	2.2	n.d.	3.4	0.03	4.6	442	88	0.37	4.1
38		Me	single isomer[b]	14	n.d.	2.6	0.58	3.7	458	97	0.33	4.1
39		Me	single isomer[b]	0.5	n.d.	3.5	0.29	4.2	472	97	0.38	5.1
40		Me	single isomer	0.4	68	3.9	0.26	4.6	486	97	0.37	4.8
41		Me	single isomer[b]	10	n.d.	0.93	0.29	3.7	444	97	0.34	4.3
42a	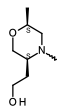	Me	single isomer[b]	4	101	2.7	2.8	3.9	458	97	0.35	4.5
42b	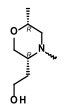	Me	single isomer[b]	6	n.d.	2.3	1.4	3.9	458	97	0.34	4.3
43	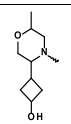	Me	single isomer[b]	2	n.d.	3.4	3.4	3.5	484	97	0.34	5.3

[a]n.d.: not determined. [b]Single isomer of unknown configuration.

https://dx.doi.org/10.1021/acs.jmedchem.0c01035
J. Med. Chem. XXXX, XXX, XXX−XXX

the PXR (Phe288 and Trp299) and the triazolopyridine core (**32**, PXR MEC = 20 μM) to diminish the hydrogen-bond strength with Gln285 in the PXR. Introduction of a methyl substituent at the benzylic P1 position increased metabolic stability somewhat. However, all compound modifications outlined in Table 2 led to a decrease in thrombin inhibition relative to **20rac**. Thus, potency had to be regained with altered P4 residues to be able to combine the promising P1 modifications and finally increase thrombin inhibition.

Optimization of the P4 Residue. The first approach toward more potent P4 residues involved substitution at position 2 of the piperidine with hydrophobic substituents of growing steric bulk to displace water molecules in the S3 pocket (Figure 4, site 34). Thrombin inhibition decreased with methyl substitution (**33**, Table 3) relative to **20a**. Ethyl and cyclopropyl (**34** and **35**) substituents gave the desired increase as these were presumably bulky enough to displace water in the S3 pocket. But since these derivatives were too lipophilic (clogP larger than 3.5), clearance was significantly increased and **35** still showed strong PXR transactivation. Addition of a second hydroxyl function to P3 resulted in the highly potent **36** (IC_{50} = 270 pM) with very low clearance but unfortunately strongly reduced Caco-2 permeation. Omitting the 4-hydroxyl group (**37a**, **37b**) led to potent, highly permeable but too lipophilic compounds with strong PXR transactivation and high metabolic clearance in rat hepatocytes. In summary, adding or omitting additional hydroxyl groups in the 4-hydroxypiperidine subseries resulted in compounds that were either too lipophilic or too hydrophilic. To reduce the granularity of polar chemical functionalities in P4, we elected to integrate an ether oxygen into the ring and limit substituents to one hydroxyl function. Thus, piperidine was exchanged by morpholine. In addition, the benzylic position was "blocked" with a methyl substituent (*R*-stereoisomer) to increase metabolic stability, as outlined above.

Substitution at position 2 of the morpholine with methyl and 2-hydroxyethyl residues gave compound **38** showing promising *in vivo* PK properties such as 38% oral bioavailability in rats (Table 5). This particular P4 residue was designed to fill the S4 pocket (Figure 4, site 1) with the methyl group and simultaneously replace a water molecule contacting the Tyr60A hydroxyl and the backbone Glu97A carbonyl oxygen (Figure 4, site 31) with the terminal hydroxyl function. Thrombin inhibition was still regarded as insufficient. Further substitution with a methyl or ethyl group at position 3 of the morpholine led to extremely potent inhibitors (**39** and **40**, 0.5 and 0.4 nM thrombin IC_{50}). **40** was cocrystallized with thrombin, with X-ray analysis confirming the stereochemistry of the most potent stereoisomer and the anticipated binding mode. Since the affinity gain from methyl to ethyl was small, we speculate that the rigidification with the additional substituent conformationally rearranges the hydroxyethyl/methyl pharmacophore in an energetically favorable way for binding. Water displacement (site 34, Figure 4) plays a minor role in this case. Unfortunately, the lipophilicity increased significantly, leading to high metabolic clearance. To reduce lipophilicity, the P4 morpholine was substituted with a methyl group at position 5 and a hydroxyalkyl residue at position 3. This functional group was expected to form a hydrogen bond with the carboxylate side chain of Thr172 or Glu217 in the S3 pocket. **40** still showed strong PXR transactivation (MEC = 0.26 μM) and weaker CYP3A4 induction in the hepatocyte assay (NOEL = 1111 ng/mL). Thrombin inhibition increased from hydroxymethyl (**41**) to hydroxyethyl (**42a**). Since both derivatives still transactivated the PXR, we designed derivatives that positioned the hydroxyl functionality rigidly in a way that would enhance binding to thrombin (hydrogen bond to Thr172, Glu217) but not to the PXR (no hydrogen bond with His407). Especially the resulting 3-hydroxycyclobutyl derivative (**43**) was a potent thrombin inhibitor (IC_{50} = 2 nM). PXR transactivation, however, was not diminished by using the rigid substituents. To further explore these results, **42a** was cocrystallized with thrombin, leading to a surprising result with respect to stereochemistry of the most active stereoisomer. The electron density clearly identified the P4 *S*,*S*-isomer **42a** as the slightly more potent (IC_{50} = 4 nM) relative to the corresponding *R*,*R*-isomer **42b** (IC_{50} = 6 nM). Isomer **42a** positions the hydroxyethyl residue in an equatorial conformation with its terminal hydroxyl group hydrogen-bonded to Tyr60A (Figure 9). An X-ray cocrystal structure of

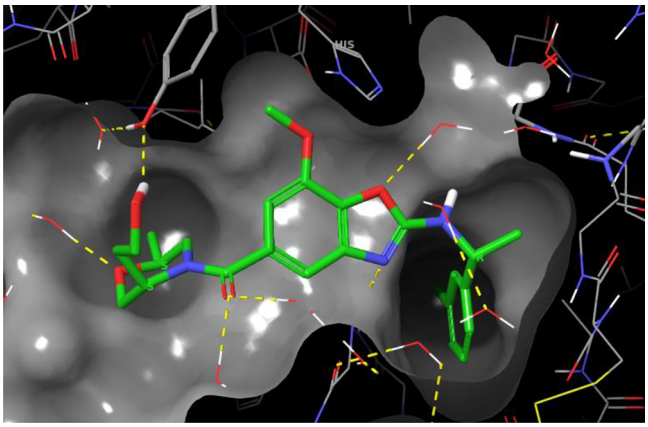

Figure 9. X-ray cocrystal structure of **42a** with thrombin (PDB code 6ZUX).

42b revealed that the *R*,*R*-isomer binds with the methyl group in the S4 pocket. Instead of hydrogen bonding to residues in the S3 pocket, the terminal hydroxyl group forms an intramolecular hydrogen bond with the compound's amide oxygen and occupies the S3 pocket (results not shown; see Table S4, Supporting Information).

Consolidating ADMET and Potency Enhancing Groups. The most potent P4 substituents were subsequently combined with somewhat more polar cores and P1 residues to address ADMET issues like clearance and CYP induction. As shown in Table 4, 4-chloro-2-pyridyl P1 derivatives (**44**, **45**, **46**) showed a reduction in PXR transactivation relative to **42a**. In the cases of **44** and **45** this also led to the desired complete loss of CYP3A4 induction as measured in the hepatocyte assay (NOEL > 10 000 ng/mL, Table 5). Thus, single modifications (e.g., of P4 or P1) that slightly decrease PXR affinity contribute synergistically. Such combinations can even lead to a significantly reduced PXR transactivation. **45**, with convincing *in vitro* pharmacokinetic properties, clearly demonstrated the success of the combination strategy. However, thrombin inhibition was still deemed to be insufficient. The other two P1 4-chloro-2-pyridyl derivatives (**44**, **46**) were potent but less attractive with respect to clearance in hepatocytes.

A similar picture emerged for combinations of the triazolopyridine core with the chlorobenzyl P1 residue (**47**, **48**, **49**). Thrombin inhibition was even weaker relative to the benzoxazole core derivatives, and PXR transactivation was

https://dx.doi.org/10.1021/acs.jmedchem.0c01035
J. Med. Chem. XXXX, XXX, XXX−XXX

Table 4. Combination of Potent P4 Residues with Core and P1 Modifications[a]

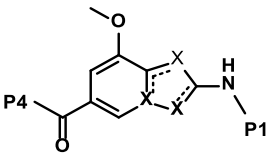

Compd	P4	Core	P1	Stereochemistry	Thrombin IC_{50} [nM]	Caco-2 flux P_{app} (A–B) [nm/s]	CL_b (hepatocytes) [L/h/kg]	PXR MEC [μM]	clogP	MW_{corr}	PSA [Å^2]	LE (with MW_{corr})	LLE (with clogP)
44	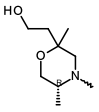			single isomer[a]	2.5	n.d.[b]	2.5	8.0	2.5	459	110	0.36	6.1
45	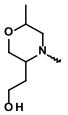			single isomer[a]	29	111	1.2	17	2.2	445	110	0.32	5.4
46	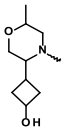			single isomer[a]	8.0	n.d.	2.7	8.2	1.8	471	110	0.31	6.3
47	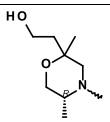			single isomer[a]	8.7	81	2.8	15	2.9	458	101	0.34	5.2
48	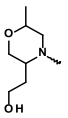			single isomer, *cis*	52	n.d.	1.9	11	2.5	444	101	0.31	4.7
49	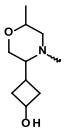			2 diastereomers	9.4	72	3.0	13	2.2	470	101	0.31	5.9
50	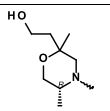		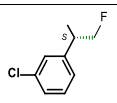	single isomer[a]	0.09	n.d.	3.4	0.39	4.0	476	97	0.39	6.1
51	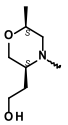		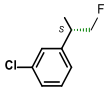	single isomer	0.7	131	1.9	1.9	3.6	462	97	0.37	5.6
52	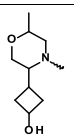		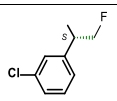	single isomer[a]	0.3	n.d.	3.4	3.0	3.2	488	97	0.34	6.3

[a]Single isomer of unknown configuration, [b]n.d.: not determined.

reduced but metabolic stability was not sufficient. **47** showed no detectable CYP3A4 induction (Table 5).

Nevertheless, with these compounds we were close to an acceptable overall pharmacokinetic profile (Table 5). However, thrombin inhibition was considered to be about 1 order of magnitude too weak. The challenge was to devise modifications that would increase thrombin binding without changing the physicochemical properties significantly. A thorough analysis of the cocrystal structure of **42a** with thrombin was performed. The binding site surface was scanned for hydrophobic and hydrogen-bond donor functionalities. The only hydrogen-bond donors in the direct vicinity of **42a** were the two backbone NH groups forming the oxyanion hole (Gly193 and Ser195). Interestingly **28**, as a mixture of eight isomers, gave a hint that positioning a trifluoromethyl group in this region led to a decrease in thrombin affinity. Molecular modeling studies helped to explain the observed effect by showing that only one fluorine atom is needed as acceptor, whereas the other two fluorines result in electrostatic repulsion. Therefore, monofluoromethyl derivatives were

https://dx.doi.org/10.1021/acs.jmedchem.0c01035
J. Med. Chem. XXXX, XXX, XXX−XXX

Table 5. *In Vivo* Pharmacokinetic Properties (iv Bolus and po Rats) and CYP3A4 Induction of Selected Compounds

Compd	MRT_{iv} [h]	AUC_{norm} [kg·h/L]	CL_b [L h^{-1} kg^{-1}]	Blood/plasma ratio	V_{ss} [L/kg]	$t_{1/2}$ [h]	$F^{b,c}$ [%]	CYP3A4 induction, NOEL[d] [ng/mL]
Dabigatran[a] (etexilate, po)	1.6	3.0	0.59	n.d.	0.54	1.2	1.9	n.d.
20a	1.1	0.48	1.7	1.24	2.4	1.3	46	370
38	1.8	0.33	2.9	1.07	5.6	2.7	38	n.d.
40	1.2	0.32	3.9	1.07	3.7	1.0	n.d.	1111
41	1.3	0.47	2.4	0.88	2.7	1.1	n.d.	n.d.
44	0.46	0.23	4.0	1.08	2.0	0.44	n.d.	>10000
45	0.51	0.39	2.4	1.08	1.3	0.5	n.d.	>10000
47	0.36	0.16	4.6	1.35	2.2	0.32	n.d.	>10000
50	1.1	0.33	3.2	0.94	3.3	1.1	n.d.	n.d.
51	1.2	0.34	3.1	0.97	3.5	1.4	38	>10000

[a]The iv experiments were performed with dabigatran (zwitterionic compound, no prodrug), and po experiments were performed with dabigatran etexilate. [b]Oral bioavailability. [c]n.d.: not determined. [d]NOEL: no effect level.

thought to be slightly more polar (compared to methyl substituents) in a position that should enhance thrombin binding and further block the benzylic position to metabolic attack. Several derivatives were prepared, and while thrombin inhibition was indeed increased by a factor of about 5 (relative to the fluorine lacking derivatives), the effects on clearance and CYP induction were not conclusive or counterproductive throughout this subseries. The binding mode of **51** was confirmed by X-ray cocrystal structural analysis and is essentially identical to **42a**, with the fluorine substituent in close vicinity to the oxyanion backbone NH groups of Gly193 (2.3 Å) and Ser195 (2.2 Å). **51** was characterized in depth.

Characterization of the Clinical Candidate 51. **51** showed convincing overall properties with subnanomolar thrombin inhibition (IC_{50} = 0.71 nM), excellent Caco-2 permeability, low plasma protein binding across species (e.g., binding of 78% in rat and human) and a moderate stability in hepatocytes and *in vivo* clearance. Although PXR transactivation was still detectable (MEC = 1.9 μM, Table 4), no CYP3A4 induction in human hepatocytes (NOEL > 10000 ng/mL, Table 5) was found. The reasons for this discrepancy are unknown. In general, a good correlation between PXR transactivation and CYP induction in hepatocytes was observed for the underlying compound class (compare Tables 4 and 5). **51** does not affect related serine proteases (such as trypsin, plasmin, tPA, FVIIa, FXa, FXIa, and plasma kallikrein) at concentrations up to 20 μM, demonstrating >10 000-fold selectivity for thrombin relative to these other homologous serine proteases. In rat, rabbit, and dog plasma, IC_{50} values of 10 nM, 20 nM, and 6.5 nM, respectively, were measured.

The prolongation of the prothrombin time (PT) and the activated partial thromboplastin time (aPTT) were measured to determine the *in vitro* anticoagulant activity of **51** (defined as the inhibitor concentration required to double the time to fibrin formation). In human plasma, the clotting times were doubled at a concentration of 1.1 μM (PT) and of 0.70 μM (aPTT).

The *in vivo* antithrombotic effects of **51** were determined in *in vivo* models for arterial and venous thrombosis after iv and po application. In the arteriovenous shunt model in anesthetized rats, **51** reduced the thrombus weight in a dose-dependent manner after iv administration (Figure 10A). When the bleeding time was determined at the tail, mild prolongation (<2-fold) was observed (Figure 10B). In another thrombosis model with venous stasis in the vena cava in rats, **51** demonstrated dose-dependent thrombus weight reduction after po administration (Figure 10C).

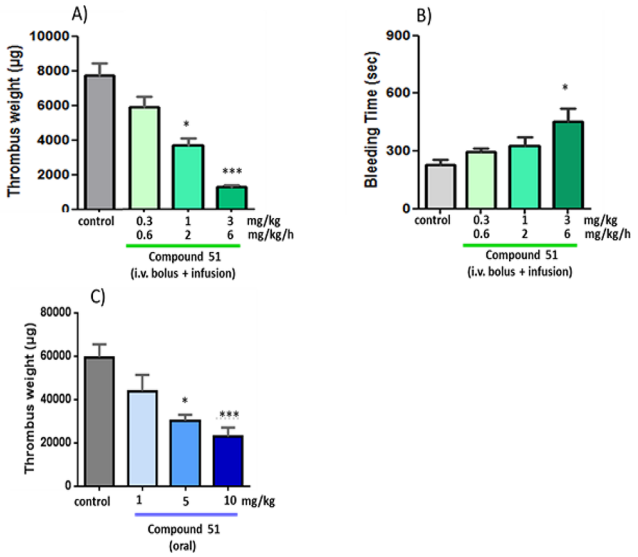

Figure 10. *In vivo* antithrombotic effects of **51** (n = 6−10, ±SEM): (A) thrombus weight reduction in an arteriovenous shunt model in rat (n = 6 ± SEM); (B) simultaneously conducted tail bleeding time model in the same animals; (C) thrombus weight reduction in a venous thrombosis model ("Wessler model") in rat; *p < 0.05, ***p < 0.0001.

Due to its overall favorable and balanced pharmacokinetic and pharmacodynamic properties, **51** (BAY1217224, Table 5) was selected for a clinical phase 1 study. Human PK was predicted using allometric scaling based on three species leading to a peak/trough ratio of 3.4 after BID dosing. Since there is no need for a prodrug approach, lower intraindividual differences are expected, and the low renal excretion rate makes it an excellent candidate for use in patients with impaired renal function, a difficult-to-treat population to date. Compound **51** was orally administered to 22 healthy volunteers in three increasing doses. Peak plasma concentrations were reached early after oral administration (t_{max} = 0.75 h) and a low-to-medium variability of AUC and C_{max} was observed. The terminal half-life ranged from 9.5 to 13 h.

https://dx.doi.org/10.1021/acs.jmedchem.0c01035
J. Med. Chem. XXXX, XXX, XXX−XXX

Scheme 1. General Synthetic Pathway for the Benzoxazole Derivatives[a]

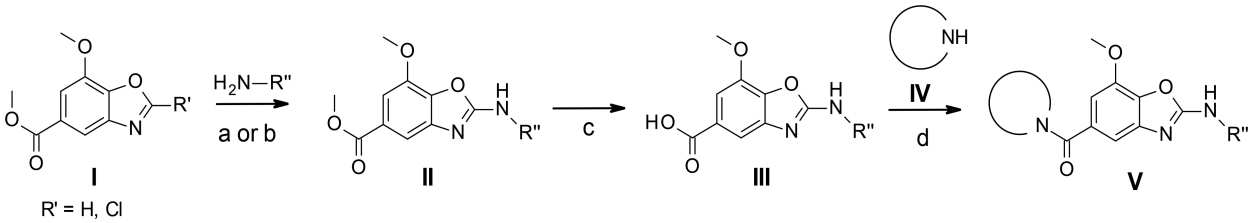

[a]Reagents and conditions: (a) R′ = H, Ag_2CO_3, benzoic acid, acetonitrile, 60 °C; (b) R′ = Cl, Hünig's base, DMF, rt; (c) 1 N NaOH, 1,4-dioxane, rt; (d) HATU, Hünig's base, DMF, rt.

CONCLUSION

The design of BAY1217224, an orally bioavailable, selective, neutral, non-prodrug thrombin inhibitor, has been described. To the best of our knowledge, this is the first molecule identified with such properties. Key to the discovery of BAY1217224 was the careful selection of the benzoxazole lead series using X-ray crystallography, computed water energetics in the substrate pocket, and evaluation of a number of different potential leads in a variety of assays. In the optimization of the benzoxazole lead series, we focused the properties of the prepared compounds to a small window of favorable physicochemical properties to balance absorption and metabolic stability. A persistent cytochrome P450 3A4 induction issue was encountered during the optimization. The problem was addressed using PXR cocrystallization, careful SAR analysis, and induced fit docking studies. Structural elements leading to decreased PXR affinity were identified and could be combined with features reinstalling thrombin inhibition. The resulting IC_{50} = 0.7 nM thrombin inhibitor BAY1217224 is highly selective and has excellent Caco-2 permeability, moderate clearance, and no CYP induction potential in hepatocytes. The compound has reached clinical trials which have confirmed oral bioavailability in healthy male volunteers.

EXPERIMENTAL SECTION

Druggability Assessment. For the modeling of oral druggability, the SiteMap[18] program was applied. Fifteen site points were required to detect a ligand binding pocket. The standard grid for site points was used, together with the more restrictive hydrophobicity definition. The Dscore was used to compare oral druggability of different serine proteases. X-ray structures were prepared using Schrödinger's Maestro protein preparation routine.[30]

Physicochemical Property Estimation. Lipophilicity of compounds was estimated using clogP.[19] Polar surface area was characterized with the tPSA[20] descriptor. The corrected molecular weight (MW_{corr})[21] was used to quantify molecule size. MW_{corr} applies appropriate weight corrections for molecules with halogens because these atoms have an unproportionally low volume compared to their atomic weight. Thus, it is a surrogate parameter for the molecular volume and related to diffusion rates.

Docking in Thrombin. Glide SP version 3.5[28] (Schrödinger LLC) was used to dock compounds into prepared thrombin X-ray structures. The X-ray structure of thrombin in complex with **10** was used for the majority of the docking studies. The ligand was placed in the center of a 22 Å box to calculate the interaction grid. The van der Waals scaling factor was set to 0.8 and the partial charge cutoff to 0.15. The ligands were docked flexibly and nonplanar amide bonds were penalized. 10 000 poses per docking run were sampled. The complex with the most probable binding pose after manual inspection of top ranked poses was energy-minimized using the OPLS2005 force field[25] (dielectric constant 1.0, constant dielectric, solvent water, Polak–Ribière conjugate gradient, convergence threshold 0.5) in MacroModel (Schrödinger LLC).

Induced Fit Docking[31] in the PXR. PXR active compounds were docked using Glide in the first step of the induced fit protocol. The X-ray structure of the PXR in complex with **17** was used for the docking experiments. To generate a diverse ensemble of ligand poses, reduced ligand and protein van der Waals radii (scaling factor 0.5) were used during the docking step. For each pose, a Prime structure prediction was then used to accommodate the ligand by reorienting nearby side chains (within a radius of 5 Å). Especially His407, Arg410, and Gln285 were treated flexibly in the docking protocol. These residues and the ligand were then energy-minimized. Each PXR active compound was re-docked into its corresponding low-energy protein conformations (energy window of 30 kcal/mol to the lowest energy conformation), and the resulting complexes were ranked according to GlideScore.

Chemistry. We describe the synthesis of **51** here in detail. Synthesis of the other derivatives (**10**, **13**–**19**, **20a**/**20b**, **21**–**26**, **27a**/**27b**, **28**–**32**, **33a**/**33b**, **34**–**36**, **37a**/**37b**, **38**–**41**, **42a**/**42b**, **43**–**50**, **52**) is described in Supporting Information or in the filed patent applications.[15,32–34] The key step in the synthesis of the benzoxazoles **V** (Scheme 1), the introduction of the benzylic amine moiety, could be successfully carried out starting from either the unsubstituted (R′ = H) or the prefunctionalized (R′ = Cl) benzoxazole **I**. In the first case, the silver-mediated direct amination methodology developed by Chang and co-workers[35] led to the desired compounds **II**, usually in moderate yield. The second possible access was the generally higher yielding S_NAr reaction via the chlorinated benzoxazole **I**.[36] Afterward, saponification of esters **II** under standard conditions resulted in high yields of the corresponding acids **III** which were then subjected to amide-coupling conditions using different cyclic secondary amines **IV** and HATU as coupling agent to obtain the final benzoxazoles **V** in good yields.

The synthesis of clinical candidate **51** (BAY1217224, Scheme 2) started from commercially available vanillic acid (**53**) which was converted in five steps and high overall yield into key building block benzoxazole **58**. The required benzylic amine **65** was produced from commercially available 3-chloroacetophenone (**59**) which was α-brominated and then subjected to a bromine–fluorine exchange to yield **61**. Reductive amination and Boc protection led to racemic **63** which was then separated into enantiomers via preparative chiral HPLC chromatography to give the desired *S*-enantiomer **64**. Finally, benzylic amine hydrochloride **65** was obtained via Boc deprotection under acidic conditions. The chiral morpholine building block **74** was synthesized starting from L-aspartic acid (**66**). After conversion into bis-methyl ester **67** and benzyl protection of the amine, reduction to diol **69** was carried out using lithium aluminum hydride. Treatment of diol **69** with 2-chloropropionyl chloride set the stage for cyclization under basic conditions to provide oxomorpholine **71**. Subsequent carbonyl reduction, separation of the diastereoisomers via HPLC, and benzyl deprotection gave the required building block **73**. Finally, reaction of benzoxazole **58** with benzylic amine **65**, followed by ester saponification and coupling with chiral secondary amine **73**, resulted in **51**.

General Procedures. All commercial reagents and catalysts were used as provided by the commercial supplier without purification.

https://dx.doi.org/10.1021/acs.jmedchem.0c01035
J. Med. Chem. XXXX, XXX, XXX–XXX

Scheme 2. Synthesis of 51 (BAY1217224)[a]

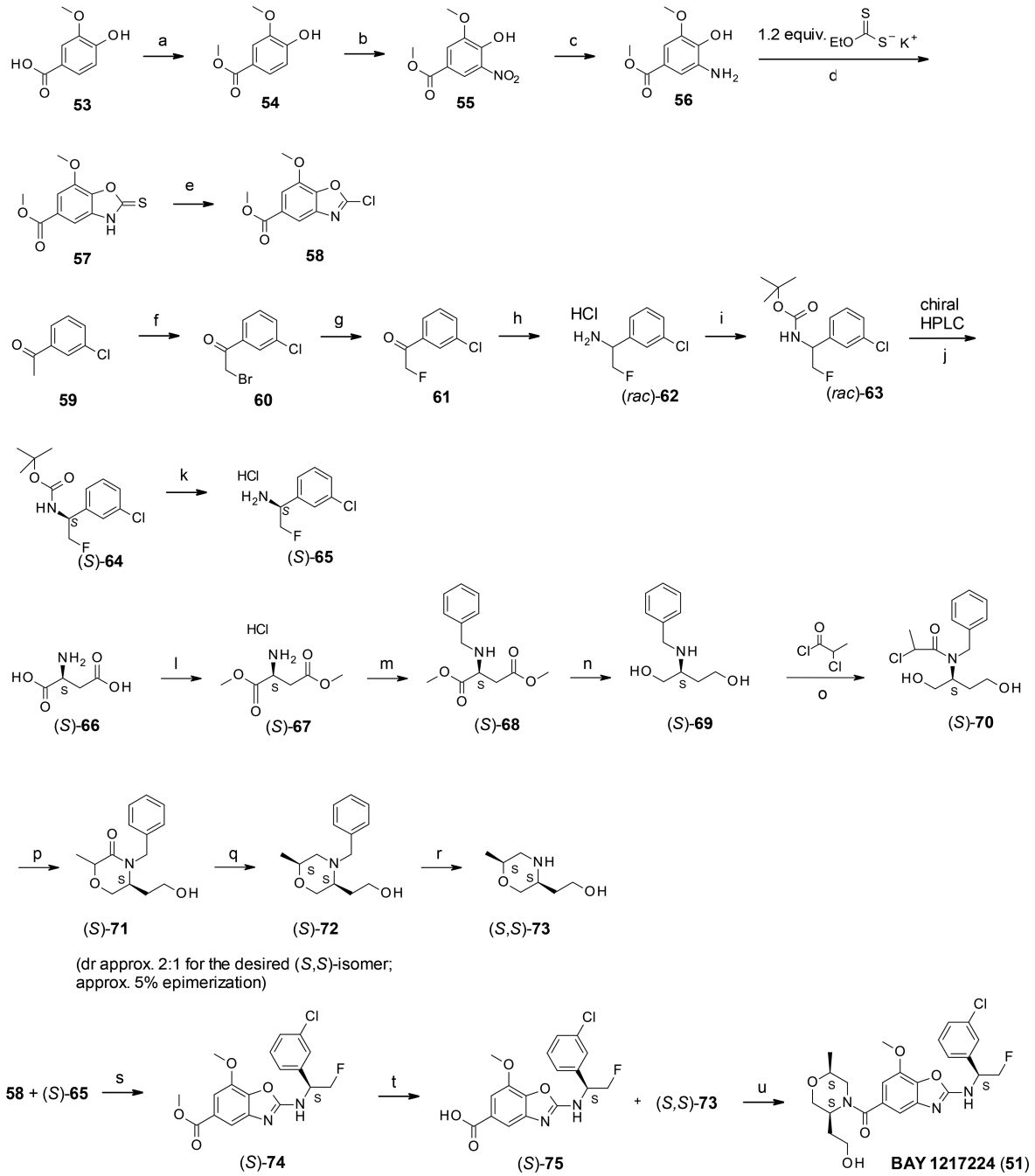

[a]Reagents and conditions: (a) $SOCl_2$, MeOH, reflux, 100%; (b) fuming HNO_3, HOAc, rt, 80%; (c) H_2 (1 bar), 10% Pd/C (5 wt %), THF/EtOH (2:1), rt, 96%; (d) pyridine, reflux, 96%; (e) $SOCl_2$, DMF (cat.), 70 °C, 82%; (f) Br_2, DCM, 82%; (g) KF, ZnF_2, TBAF·3 H_2O, acetonitrile, 80 °C, 58% or Selectfluor, MeOH, 110 °C, microwave, 86%; (h) (i) NH_3, Ti(O*i*-Pr)$_4$, EtOH, rt, (ii) $NaBH_4$, (iii) 4 N HCl in 1,4-dioxane, 1,4-dioxane, rt; (i) Boc_2O, triethylamine, DCM, rt; (j) chiral chromatography, 23% over five steps; (k) 4 N HCl in 1,4-dioxane, 1,4-dioxane, rt, 100%; (l) $SOCl_2$, MeOH, reflux; (m) benzaldehyde, $NaBH(OAc)_3$, triethylamine, DCM, 50% over two steps; (n) $LiAlH_4$, THF, reflux, 78%; (o) triethylamine, *i*-PrOH, 0 °C, 90%; (p) KO*t*-Bu, *i*-PrOH, 0 °C to rt, 90%; (q) borane−dimethyl sulfide, THF, rt; (r) H_2 (1 bar), 10% Pd/C (5 wt %), 20% $Pd(OH)_2$/C (5 wt %), EtOH, 99%; (s) Hünig's base, DMF, rt, 92%; (t) 1 N NaOH, 1,4-dioxane, rt, 88%; (u) HATU, Hünig's base, DMF, rt, 70%.

Solvents for synthesis, extraction, and chromatography were reagent grade and used as received. Moisture-sensitive reactions were carried out under an atmosphere of argon, and anhydrous solvents were used as provided by the commercial supplier. ^{1}H NMR spectra were recorded on Bruker Avance spectrometers operating at 400 MHz. Chemical shifts (δ) are reported in ppm relative to TMS as an internal standard. The descriptions of the coupling patterns of ^{1}H NMR signals are based on the optical appearance of the signals and do not necessarily reflect the physically correct interpretation. In general, the chemical shift information refers to the center of the signal. LC−MS analysis was performed using the respective methods 1a−5a, as noted. Unless otherwise indicated, all compounds have ≥95% purity.

Method 1a. Instrument: Waters ACQUITY SQD UPLC system; column, Waters Acquity UPLC HSS T3 1.8 μm, 50 mm × 1 mm; mobile phase A, 1 L of water + 0.25 mL of 99% strength formic acid; mobile phase B, 1 L of acetonitrile + 0.25 mL of 99% strength formic

https://dx.doi.org/10.1021/acs.jmedchem.0c01035
J. Med. Chem. XXXX, XXX, XXX−XXX

acid; gradient, 0.0 min 90% A → 1.2 min 5% A → 2.0 min 5% A; oven, 50 °C; flow rate, 0.40 mL/min; UV detection, 208−400 nm.

Method 2a. Instrument, Micromass Quattro Premier with Waters UPLC Acquity; column, Thermo Hypersil GOLD 1.9 μm, 50 mm × 1 mm; mobile phase A, 1 L of water + 0.5 mL of 50% strength formic acid; mobile phase B, 1 L of acetonitrile + 0.5 mL of 50% strength formic acid; gradient, 0.0 min 97% A → 0.5 min 97% A → 3.2 min 5% A → 4.0 min 5% A; oven, 50 °C; flow rate, 0.3 mL/min; UV detection, 210 nm.

Method 3a. MS instrument, Waters (Micromass) Quattro Micro; HPLC instrument, Agilent 1100 series; column, YMC-Triart C18 3 μm, 50 mm × 3 mm; mobile phase A, 1 L of water + 0.01 mol of ammonium carbonate; mobile phase B, 1 L of acetonitrile; gradient, 0.0 min 100% A → 2.75 min 5% A → 4.5 min 5% A; oven, 40 °C; flow rate, 1.25 mL/min; UV detection, 210 nm.

Method 4a. MS instrument, Waters (Micromass) QM; HPLC instrument, Agilent 1100 series; column, Agient ZORBAX Extend-C18 3.5 μm, 3.0 mm × 50 mm; mobile phase A, 1 L of water + 0.01 mol of ammonium carbonate, mobile phase B, 1 L of acetonitrile; gradient, 0.0 min 98% A → 0.2 min 98% A → 3.0 min 5% A → 4.5 min 5% A; oven, 40 °C; flow rate, 1.75 mL/min; UV detection, 210 nm.

Method 5a. Instrument, Waters ACQUITY SQD UPLC system; column, Waters Acquity UPLC HSS T3 1.8 μm, 50 mm × 1 mm; mobile phase A, 1 L of water + 0.25 mL of 99% strength formic acid, mobile phase B, 1 L of acetonitrile + 0.25 mL of 99% strength formic acid; gradient, 0.0 min 95% A → 6.0 min 5% A → 7.5 min 5% A; oven, 50 °C; flow rate, 0.35 mL/min; UV detection, 210−400 nm. GC−MS analysis was performed using the respective methods 1b and 2b, as noted.

Method 1b. Instrument, Thermo DFS, Trace GC Ultra; column, Restek RTX-35, 15 m × 200 μm × 0.33 μm; constant helium flow rate, 1.20 mL/min; oven, 60 °C; inlet, 220 °C; gradient, 60 °C, 30 °C/min → 300 °C (maintained for 3.33 min).

Method 2b. Instrument, Micromass GCT, GC6890; column, Restek RTX-35, 15 m × 200 μm × 0.33 μm; constant helium flow rate, 0.88 mL/min; oven, 70 °C; inlet, 250 °C; gradient, 70 °C, 30 °C/min → 310 °C (maintained for 3 min).

Method 1c. MS analysis was performed using method 1c. Instrument, Thermo Fisher-Scientific DSQ; chemical ionization; reactant gas, ammonia; source temperature, 200 °C; ionization energy 70 eV. Preparative enantiomer/diastereomer separation on a chiral phase was performed using the respective methods 1d and 2d, as noted.

Method 1d. Phase, Daicel Chiralpak AD-H SFC, 10 μm 250 mm × 20 mm, mobile phase, carbon dioxide/ethanol 70:30; flow rate, 100 mL/min, makeup flow rate, 30 mL/min, backpressure, 80 bar; temperature, 40 °C; UV detection, 220 nm.

Method 2d. Phase, Daicel Chiralpak AY-H, 5 μm 250 mm × 20 mm, mobile phase, isohexane/ethanol 90:10; flow rate, 40 mL/min; temperature, 40 °C; UV detection, 220 nm. Analytical enantiomer/diastereomer separation on a chiral phase was performed using the respective methods 1e and 2e, as noted.

Method 1e. Phase, Daicel Chiralpak AS-H, 5 μm 250 mm × 4.6 mm, mobile phase, isohexane/isopropanol 50:50; flow rate, 1 mL/min; temperature, 30 °C; UV detection, 220 nm.

Method 2e. Phase, Daicel Chiralpak AD-H SFC, 5 μm 250 mm × 4.6 mm, mobile phase, carbon dioxide/ethanol 70:30; flow rate, 3 mL/min; temperature, 30 °C; UV detection, 220 nm. Assessment of optical rotation [α] was performed using an Anton Paar polarimeter MCP200 with parameters (solvent, wavelength, temperature) as indicated. Preparative normal phase chromatography (column chromatography/flash chromatography/MPLC) was performed using Biotage Isolera chromatography systems with Biotage silica cartridges or silica gel 60 (230−400 mesh) in combination with glass columns/frits.

Methyl 4-Hydroxy-3-methoxybenzoate (54). 4-Hydroxy-3-methoxybenzoic acid **53** (60.0 g, 357 mmol) in methanol (500 mL) was treated at 0 °C dropwise with thionyl chloride (91.1 mL, 1.25 mol, 3.5 equiv). After complete addition, the solution was stirred under reflux for 2 h. The reaction mixture was concentrated under reduced pressure to afford **54** which was used without further purification within the next step. Yield: 65.0 g (100%). ^{1}H NMR (400 MHz, DMSO-d_6): δ = 9.97 (br s, 1H), 7.31−7.55 (m, 2H), 6.86 (d, J = 8.1 Hz, 1H), 3.81 (s, 3H), 3.79 (s, 3H). LC−MS (method 2a): t_R (min) = 0.78. MS (ESI+): m/z = 183 $[M + H]^+$.

Methyl 4-Hydroxy-3-methoxy-5-nitrobenzoate (55). Methyl 4-hydroxy-3-methoxybenzoate **54** (320.0 g, 1.70 mol) in conc acetic acid (1.00 L) was treated at 20 °C (slight ice cooling) dropwise with 65% nitric acid (177 mL, 2.56 mol, 1.5 equiv) [**CAUTION**: reaction exhibits a very slow exotherm which can lead to a severe run-away reaction due to accumulation. Therefore, the reaction temperature should always be monitored and kept at or below 20 °C]. After complete addition, the mixture was stirred for another 15 min until completion. The formed suspension was filtered under reduced pressure and the solid was washed with water to afford after drying under reduced pressure **55** which was used without further purification within the next step. Yield: 290 g (73%). ^{1}H NMR (400 MHz, DMSO-d_6): δ = 11.43 (br s, 1H), 8.02 (d, J = 2.0 Hz, 1H), 7.66 (d, J = 2.0 Hz, 1H), 3.95 (s, 3H), 3.86 (s, 3H). LC−MS (method 1a): t_R (min) = 0.83. MS (ESI+): m/z = 226 $[M + H]^+$.

Methyl 3-Amino-4-hydroxy-5-methoxybenzoate (56). Methyl 4-hydroxy-3-methoxy-5-nitrobenzoate **55** (50.0 g, 220 mmol) in methanol (1.00 L) and THF (500 mL) was treated with 10% Pd/C (4.73 g) and then stirred for 48 h under 1 atm of hydrogen. The reaction mixture was filtered over Celite under vacuum and the filtrate was concentrated under reduced pressure to afford **56** which was used without further purification within the next step. Yield: 42.5 g (96%). ^{1}H NMR (400 MHz, DMSO-d_6): δ = 9.97 (br s, 1H), 7.31−7.55 (m, 2H), 6.86 (d, J = 8.1 Hz, 1H), 3.81 (s, 3H), 3.79 (s, 3H). LC−MS (method 1a): t_R (min) = 0.46. MS (ESI+): m/z = 197 $[M + H]^+$.

Methyl 7-Methoxy-2-thioxo-2,3-dihydro-1,3-benzoxazole-5-carboxylate (57). Methyl 3-amino-4-hydroxy-5-methoxybenzoate (20.0 g, 101 mmol) and potassium *O*-ethyl dithiocarbonate (17.9 g, 112 mmol, 1.1 equiv) were dissolved in pyridine (400 mL), and the solution was stirred under reflux for 3 h (analogously to[36]). The reaction mixture was then cooled and poured onto a mixture of ice (600 g) and concentrated aqueous hydrogen chloride solution (60 mL). The solid formed was filtered off under reduced pressure and washed with water (5 × 200 mL). The solid was dried initially at 50 °C/40 mbar and then under high vacuum to afford **57**. Yield: 23.3 g (96%). ^{1}H NMR (400 MHz, DMSO-d_6): δ = 14.1 (br s, 1H), 7.45 (d, J = 1.0 Hz, 1H), 7.32 (d, J = 1.2 Hz, 1H), 4.00 (s, 3H), 3.88 (s, 3H). LC−MS (method 1a): t_R (min) = 0.79. MS (ESI+): m/z = 240 $[M + H]^+$.

Methyl 2-Chloro-7-methoxy-1,3-benzoxazole-5-carboxylate (58). 7-Methoxy-2-thioxo-2,3-dihydro-1,3-benzoxazole-5-carboxylate (150 g, 627 mmol) was suspended in thionyl chloride (450 mL), catalytic amounts of *N*,*N*-dimethylformamide (1.0 mL) were added, and the mixture was then stirred for 3 h (analogously to ref 36). More *N*,*N*-dimethylformamide (1.0 mL) was added, and the mixture was stirred at 70 °C until the evolution of gas had ceased (about 4 h). The reaction solution was concentrated under reduced pressure, and the residue was coevaporated with dichloromethane (3 × 200 mL) to completely remove the thionyl chloride. The solid was dried under high vacuum and then purified by column chromatography on silica gel (dichloromethane). Alternatively, the crude product can also be used further directly. Yield: 125.6 g (82%). ^{1}H NMR (400 MHz, chloroform-*d*): δ = 7.99 (d, J = 1.3 Hz, 1H), 7.62 (d, J = 1.2 Hz, 1H), 4.07 (s, 3H), 3.96 (s, 3H). LC−MS (method 1a): t_R (min) = 1.00. MS (ESI+): m/z = 242 $[M + H]^+$.

2-Bromo-1-(3-chlorophenyl)ethanone (60). 1-(3-Chlorophenyl)ethanone (126 mL, 970 mmol) in dichloromethane (1.10 L) was treated at 20−25 °C dropwise with a solution of bromine (49.8 mL, 970 mmol, 1.0 equiv) in dichloromethane (300 mL). After stirring for 30 min, ice-cold water (600 mL) was added to the reaction mixture. After extraction and phase separation, the organic layer was dried over sodium sulfate, filtered, and concentrated under reduced pressure. The residue was dissolved in *tert*-butyl methyl ether (150 mL) and then treated with *n*-heptane (1.00 L). The

https://dx.doi.org/10.1021/acs.jmedchem.0c01035
J. Med. Chem. XXXX, XXX, XXX−XXX

solution was cooled under stirring to −10 °C, the precipitated solid was filtered under reduced pressure and the residue washed with cold *n*-heptane (100 mL). The solid was dried initially under high vacuum to afford **60**. Yield: 166 g (73%). ^{1}H NMR (400 MHz, DMSO-d_6): δ = 8.03 (t, J = 1.8 Hz, 1H), 7.93−7.98 (m, 1H), 7.76 (ddd, J = 0.9, 2.1, 8.0 Hz, 1H), 7.54−7.64 (m, 1H), 4.99 (s, 2H). LC−MS (method 2a): t_R (min) = 2.29. MS (ESI+): m/z = 233 $[M + H]^+$.

1-(3-Chlorophenyl)-2-fluoroethanone (61). *Method 1.* Tetra-*n*-butylammonium fluoride trihydrate (50.7 g, 161 mmol), zinc fluoride (22.1 g, 214 mmol), and potassium fluoride (6.22 g, 107 mmol) were initially charged in acetonitrile (850 mL) and stirred at 80 °C for 1 h (analogously to ref 37). 2-Bromo-1-(3-chlorophenyl)-ethanone **60** (50.0 g, 214 mmol) in acetonitrile (210 mL) was then added dropwise at this temperature over a period of 3 h, and the mixture was subsequently stirred at 80 °C for a further 3 h. The reaction solution was cooled to room temperature, and the precipitated salts were filtered off over a glass frit. The filtrate was concentrated under reduced pressure, water was added to the residue, and the mixture was extracted repeatedly with *tert*-butyl methyl ether. Further precipitated salts were removed by filtration. The organic phases were dried over magnesium sulfate, filtered, and concentrated under reduced pressure. The crude product was then purified by flash chromatography on silica gel (petroleum ether/ethyl acetate 10:1) to afford **61**. Yield: 27.0 g (58%, purity 80%). ^{1}H NMR (400 MHz, DMSO-d_6): δ = 7.91 (t, J = 1.7 Hz, 1H), 7.85 (d, J = 7.8 Hz, 1H), 7.73−7.80 (m, 1H), 7.55−7.63 (m, 1H), 5.84 (d, J = 45.9 Hz, 2H). GC−MS (method 1B): t_R (min) = 3.73. MS (EI+): m/z = 172 $[M]^+$.

Method 2. 1-(Chloromethyl)-4-fluoro-1,4-diazoniabicyclo[2.2.2]-octane bistetrafluoroborate (Selectfluor) (45.8 g, 129 mmol) was added to 1-(3-chlorophenyl)ethanone (10.0 g, 64.7 mmol) in methanol (80.0 mL) and then, in 10 portions, stirred in the microwave (Biotage Synthesizer) at 110 °C for 2.5 h (analogously to ref 38). Water (5 mL) was then added to each portion, and the portions were stirred in the microwave at 110 °C for 1 h. The reaction mixtures were then combined, the methanol was removed under reduced pressure, and the residue was diluted with water and then extracted with ethyl acetate. The organic phase was dried over sodium sulfate, filtered, and concentrated under reduced pressure. The crude product was used for the next step without further purification. Yield: 12.5 g (86%, purity 77%). GC−MS (method 2b): t_R (min) = 3.56. MS (EI+): m/z = 172 $[M]^+$.

***rac*-1-(3-Chlorophenyl)-2-fluoroethanamine Hydrochloride (62).** *Method 1.* Under an atmosphere of argon, titanium tetraisopropoxide (6.52 g, 6.87 mL, 23.0 mmol) was added to 1-(3-chlorophenyl)-2-fluoroethanone **61** (2.00 g, 11.5 mmol) in 2 M ethanolic ammonia solution (28.7 mL, 57.4 mmol), and the mixture was stirred at room temperature for 16 h. Afterward, sodium borohydride (654 mg, 17.3 mmol) was added and the mixture was stirred at room temperature for 5 h. Further sodium borohydride (350 mg, 9.25 mmol) was added, and the mixture was stirred at room temperature overnight. The reaction solution was poured into 25% strength aqueous ammonia solution (100 mL) and then filtered through Celite. *tert*-Butyl methyl ether (200 mL) was added to the filtrate, and the mixture was extracted. After phase separation, the aqueous phase was extracted with *tert*-butyl methyl ether (100 mL). The combined organic phases were dried over sodium sulfate, filtered, and concentrated under reduced pressure. The crude product was dissolved in diethyl ether/tetrahydrofuran (5:1; 60 mL), and a 4 N solution of hydrogen chloride in 1,4-dioxane (10.0 mL) was then added. The solid formed was filtered off under reduced pressure, washed with a little diethyl ether, and dried under high vacuum. Yield: 1.54 g (63%). ^{1}H NMR (400 MHz, DMSO-d_6): δ = 8.98 (br s, 3H), 7.70 (s, 1H), 7.60−7.47 (m, 3H), 4.88−4.67 (m, 3H). LC−MS (method 4a): t_R (min) = 1.94. MS (ESI+): m/z = 174 $[M + H - HCl]^+$.

Method 2. Titanium tetraisopropoxide (1.10 kg, 1.16 L, 3.88 mol) was added dropwise to 1-(3-chlorophenyl)-2-fluoroethanone **61** (335 g, 1.94 mol) in 2 M ethanolic ammonia solution (4.85 L, 9.71 mol) (the temperature was kept at 20 °C by ice cooling), and the mixture was stirred at room temperature overnight. At 10 °C, sodium borohydride (110 g, 2.91 mol) was added in four portions, and the mixture was stirred at room temperature for 36 h. Further sodium borohydride (29.4 g, 776 mmol) was added, and the mixture was stirred at room temperature for 1 h. The reaction solution was poured into 2 M aqueous ammonia solution (4.85 L), and the precipitated salts were then filtered off over a frit under reduced pressure. *tert*-Butyl methyl ether (14 L) and water (50 L) were added to the filtrate, the mixture was extracted, and 5% aqueous sodium chloride solution was then added to facilitate phase separation. After phase separation, the aqueous phase was re-extracted with *tert*-butyl methyl ether (5 L) and the combined organic phases were dried over sodium sulfate, filtered, and concentrated under reduced pressure. The crude product was dissolved in diethyl ether/tetrahydrofuran (10:1; 1.1 L), and a 4 N solution of hydrogen chloride in 1,4-dioxane (385 mL) was then added with stirring and ice cooling. The precipitated white solid was filtered off under reduced pressure, washed with a little diethyl ether, and dried under high vacuum. Yield: 261 g (77%). LC−MS (method 4a): t_R (min) = 1.93. MS (ESI+): m/z = 174 $[M + H - HCl]^+$.

***rac*-*tert*-Butyl [1-(3-Chlorophenyl)-2-fluoroethyl]carbamate (63).** *Method 1.* *rac*-1-(3-Chlorophenyl)-2-fluoroethanamine **62** (7.47 g, 43.3 mmol) was suspended in dichloromethane (150 mL). First triethylamine (9.14 g, 12.6 mL, 90.4 mmol) and then di-*tert*-butyl dicarbonate (10.3 g, 47.3 mmol) were added, and the mixture was stirred at room temperature overnight. The reaction solution was then washed with 0.5 N aqueous hydrogen chloride solution (100 mL), saturated aqueous sodium bicarbonate solution (100 mL), and water (100 mL). The organic phase was dried over sodium sulfate, filtered, and concentrated under reduced pressure. The crude product was purified by preparative RP-HPLC (water/acetonitrile). Yield: 7.23 g (61%). ^{1}H NMR (400 MHz, DMSO-d_6): δ = 7.72 (br d, J = 8.6 Hz, 1H), 7.25−7.51 (m, 4H), 4.76−5.00 (m, 1H), 4.45−4.61 (m, 1H), 4.30−4.44 (m, 1H), 1.38 (s, 9H). LC−MS (method 1a): t_R (min) = 1.10. MS (ESI+): m/z = 218 $[M + H - C_4H_9]^+$.

Method 2. Under an atmosphere of argon, *rac*-1-(3-chlorophenyl)-2-fluoroethanamine **62** (41.5 g, 198 mmol) was suspended in dichloromethane (200 mL), and subsequently first triethylamine (80.0 g, 110 mL, 790 mmol) and then dichloromethane (200 mL) were added. Afterward, di-*tert*-butyl dicarbonate (31.0 g, 142 mmol) in dichloromethane (100 mL) was added, and the mixture was stirred at room temperature overnight. Further di-*tert*-butyl dicarbonate (9.91 g, 45.4 mmol) was added, and the mixture was stirred until conversion was almost complete (monitored by TLC). The reaction solution was washed with 1 N aqueous hydrogen chloride solution (2 × 100 mL) and saturated aqueous sodium bicarbonate solution (100 mL). The organic phase was dried over sodium sulfate, filtered, and concentrated under reduced pressure. Yield: 51.0 g (94%). LC−MS (method 5a): t_R (min) = 3.25. MS (ESI+): m/z = 218 $[M + H - C_4H_9]^+$.

***tert*-Butyl [(1*S*)-1-(3-Chlorophenyl)-2-fluoroethyl]carbamate (64).** Enantiomer separation on a chiral phase of 7.23 g of the compound (*rac*)-**63** according to method 2d gave 3.05 g of enantiomerically pure (*R*)-isomer and 3.05 g of enantiomerically pure (*S*)-isomer (**64**). (*R*)-isomer: ^{1}H NMR (400 MHz, DMSO-d_6): δ = 7.72 (br d, J = 8.7 Hz, 1H), 7.45 (s, 1H), 7.26−7.41 (m, 2H), 7.26−7.30 (m, 1H), 4.81−4.97 (m, 1H), 4.45−4.57 (m, 1H), 4.32−4.44 (m, 1H), 1.19−1.46 (m, 9H). HPLC (method 1e): t_R (min) = 5.01, 99.0% ee. LC−MS (method 5a): t_R (min) = 3.26. MS (ESI+): m/z = 218 $[M + H - C_4H_9]^+$. (*S*)-isomer (**64**): ^{1}H NMR (400 MHz, DMSO-d_6): δ = 7.72 (br d, J = 8.56 Hz, 1H), 7.45 (s, 1H), 7.30−7.40 (m, 3H), 4.80−4.98 (m, 1H), 4.45−4.58 (m, 1H), 4.32−4.44 (m, 1H), 1.20−1.44 (m, 9H). HPLC (method 1e): t_R (min) = 7.46, 99.0% ee. LC−MS (method 7A): t_R (min) = 3.26. MS (ESI+): m/z = 218 $[M + H - C_4H_9]^+$.

(1*S*)-1-(3-Chlorophenyl)-2-fluoroethanamine Hydrochloride (65). (*S*)-*tert*-Butyl [1-(3-chlorophenyl)-2-fluoroethyl]carbamate (**64**) (17.3 g, 63.2 mmol) was initially charged in 1,4-dioxane (50 mL), and 4 N hydrogen chloride solution in 1,4-dioxane (79 mL, 316 mmol) was then added at room temperature. A solid formed after a short period of time. 1,4-Dioxane (250 mL) and then 4 N hydrogen chloride solution in 1,4-dioxane (31.6 mL, 126 mmol) were added,

https://dx.doi.org/10.1021/acs.jmedchem.0c01035
J. Med. Chem. XXXX, XXX, XXX−XXX

and the mixture was stirred at room temperature overnight. The suspension formed was concentrated completely under reduced pressure, the residue was triturated with *tert*-butyl methyl ether (200 mL), filtered, and the filter residue was washed with *tert*-butyl methyl ether (2 × 50 mL). The solid formed was dried under high vacuum. Yield: 13.2 g (99%). ^{1}H NMR (400 MHz, DMSO-d_6): δ = 8.91 (br s, 3H), 7.68 (s, 1H), 7.39−7.59 (m, 3H), 4.64−4.93 (m, 3H). Optical rotation: = 27.06° (c = 0.51, methanol). LC−MS (method 4a): t_R (min) = 1.94. MS (ESI+): m/z = 174 $[M + H]^+$.

Dimethyl L-Aspartate Hydrochloride (67). L-Aspartic acid (1.00 kg, 7.51 mol) in MeOH (6.00 L) was treated dropwise with thionyl chloride (1.20 L, 16.5 mol) at 0 °C (addition time: 1 h). Afterward, the reaction mixture was stirred for 7 h under reflux. The reaction mixture was then concentrated under reduced pressure, and the crude product was used for the next step without further purification. Yield: 1.50 kg (100%). ^{1}H NMR (400 MHz, DMSO-d_6): δ = 8.40−8.82 (m, 3H), 4.17−4.43 (m, 1H), 3.74 (s, 3H), 3.66 (s, 3H), 2.89−3.10 (m, 2H). GC−MS (method 1b): t_R (min) = 3.25. MS (method 1c): m/z = 162 $[M + H]^+$.

Dimethyl *N*-Benzyl-L-aspartate (68). Dimethyl L-aspartate hydrochloride **67** (375 g, 1.90 mol) in dichloromethane (4.80 L) was treated at room temperature with benzaldehyde (183 mL, 1.80 mol, 0.95 equiv) and triethylamine (264 mL, 1.90 mol, 1.00 equiv) and stirred for 2 h. Afterward, sodium triacetoxyborohydride (482 g, 2.27 mol, 1.20 equiv) was added at 0 °C and the reaction mixture was stirred at room temperature overnight. The reaction mixture was washed with 2 N aqueous hydrogen chloride solution (3 × 1.0 L), and then the aqueous phase was adjusted to pH = 8−9 with 50% aqueous sodium hydroxide solution. The aqueous phase was extracted with ethyl acetate (2 × 1.0 L), and the organic phase was dried over sodium sulfate, filtered, and concentrated under reduced pressure. The crude product was used for the next step without further purification. Yield: 288 g (61%). ^{1}H NMR (400 MHz, DMSO-d_6): δ = 7.14−7.36 (m, 5H), 3.73−3.82 (m, 1H), 3.63 (s, 3H), 3.47−3.60 (m, 4H), 3.27−3.38 (m, 1H), 2.66−2.75 (m, 1H), 2.56−2.64 (m, 1H). LC−MS (method 1a): t_R (min) = 0.45. MS (ESI+): m/z = 251 $[M + H]^+$.

(2*S*)-2-(Benzylamino)butane-1,4-diol (69). Dimethyl *N*-benzyl-L-aspartate **68** (69.0 g, 275 mmol) in tetrahydrofuran (1.00 L) was treated at 0 °C with 2.4 N lithium aluminum hydride in tetrahydrofuran (330 mL, 792 mmol, 2.88 equiv). After complete addition, the reaction mixture was stirred for 2 h under reflux. Afterward, the reaction mixture was quenched dropwise at 0 °C with water (30 mL), then with 15% aqueous sodium hydroxide solution (30 mL), and finally with water (90 mL). After 15 min, sodium sulfate (100 g) was added and the reaction mixture was stirred for another 15 min. The reaction mixture was filtered under reduced pressure, and the residue was washed with tetrahydrofuran (250 mL) and hot isopropanol (500 mL). The combined filtrates were concentrated under reduced pressure, and the crude product was used for the next step without further purification. ^{1}H NMR (400 MHz, DMSO-d_6): δ = 7.10−7.37 (m, 5H), 4.50 (br s, 1H), 3.72 (d, J = 1.5 Hz, 2H), 3.50 (dt, J = 2.57, 6.4 Hz, 2H), 3.37−3.44 (m, 1H), 3.34 (s, 3H), 2.57−2.65 (m, 1H), 1.43−1.60 (m, 2H). LC−MS (method 4a): t_R (min) = 1.82. MS (ESI+): m/z = 195 $[M + H]^+$.

***N*-Benzyl-2-chloro-*N*-[(2*S*)-1,4-dihydroxybutan-2-yl]-propanamide (70).** (2*S*)-2-(Benzyl-amino)butane-1,4-diol **69** (45.1 g, 199 mmol, purity 86%) was initially charged in isopropanol (1.00 L), the mixture was cooled to 0 °C, and triethylamine (40.2 g, 55.4 mL, 397 mmol) was added. Afterward, (*rac*)-2-chloropropionyl chloride (37.8 g, 29.6 mL, 298 mmol) was added dropwise. After 30 min of stirring, further (*rac*)-2-chloropropionyl chloride (18.9 g, 14.8 mL, 149 mmol) was added dropwise, and the reaction solution was allowed to warm to room temperature and then concentrated under reduced pressure. The residue was taken up in ethyl acetate (1.00 L) and washed with water. The organic phase was dried over sodium sulfate, filtered, and concentrated under reduced pressure. The crude product was used for the next step without further purification. Yield: 71.8 g (quant, purity 82%, diastereomer ratio about 1:1). LC−MS (method 1a): t_R (min) = 0.65 (diastereomer 1), t_R (min) = 0.67 (diastereomer 2). MS (ESI+): m/z = 286 $[M + H]^+$.

(5*S*)-4-Benzyl-5-(2-hydroxyethyl)-2-methylmorpholin-3-one (71). *N*-Benzyl-2-chloro-*N*-[(2*S*)-1,4-dihydroxybutan-2-yl]-propanamide **71** (71.8 g, 206 mmol, purity 82%) was initially charged in isopropanol (1.30 L), and the mixture was cooled to 0 °C. Afterward, potassium *tert*-butoxide (92.4 g, 824 mmol) was added in one portion, and the mixture was stirred at 0 °C for 30 min. The reaction solution was allowed to warm to room temperature, and the isopropanol was removed under reduced pressure. The residue was taken up in ethyl acetate (500 mL). Water (600 mL) was added, the mixture was extracted, and after phase separation, the aqueous phase was extracted with ethyl acetate (2 × 300 mL). The organic phases were dried over sodium sulfate, filtered, and concentrated under reduced pressure. The crude product was used for the next step without further purification. Yield: 58.6 g (quant, purity 90%, diastereomer ratio about 3:2). LC−MS (method 2a): t_R (min) = 1.51 (diastereomer 1), t_R (min) = 1.53 (diastereomer 2). MS (ESI+): m/z = 250 $[M + H]^+$.

2-[(3*S*,6*S*)-4-Benzyl-6-methylmorpholin-3-yl]ethanol (72). (5*S*)-4-Benzyl-5-(2-hydroxyethyl)-2-methylmorpholin-3-one **72** (30.0 g, 108 mmol) was initially charged in tetrahydrofuran (1.10 L), 2 M borane−dimethyl sulfide complex solution in tetrahydrofuran (217 mL, 433 mmol) was added under argon, and the mixture was stirred under reflux for 2 h. The mixture was subsequently cooled to 0 °C, methanol (200 mL) was added carefully, and the mixture was stirred under reflux for 30 min. The mixture was subsequently concentrated completely under reduced pressure, and the residue was taken up in acetonitrile and subjected to purification and diastereomer separation by preparative RP-HPLC (acetonitrile/water, isocratic). Here, the target compound eluted as second component, (3*S*,6*S*)-diastereoisomer 2. Yield: 12.1 g (47%); (3*S*,6*R*)-diastereoisomer 1. Yield: 6.23 g (24%).

(3S,6S)-Diastereoisomer 2. ^{1}H NMR (400 MHz, DMSO-d_6): = δ 7.13−7.39 (m, 5H), 4.42 (t, J = 5.1 Hz, 1H), 3.36−3.72 (m, 7H), 2.56−2.64 (m, 1H), 2.27−2.36 (m, 1H), 2.14−2.26 (m, 1H), 1.60−1.84 (m, 2H), 1.00 (d, J = 6.11 Hz, 3H). LC−MS (method 3a): t_R (min) = 2.33 min. MS (ESI+): m/z = 236 $[M + H]^+$.

(3S,6R)-Diastereoisomer 1. ^{1}H NMR (400 MHz, DMSO-d_6): δ = 7.07−7.50 (m, 5H), 4.49 (t, J = 5.0 Hz, 1H), 4.10 (d, J = 13.69 Hz, 1H), 3.76 (dd, J = 3.4, 11.3 Hz, 1H), 3.37−3.57 (m, 3H), 3.21−3.33 (m, 1H), 2.95 (d, J = 13.5 Hz, 1H), 2.27 (dt, J = 3.55, 7.03 Hz, 1H), 1.80 (dtd, J = 2.6, 7.2, 14.3 Hz, 1H), 1.68 (dd, J = 10.4, 11.4 Hz, 1H), 1.48 (qd, J = 7.0, 13.9 Hz, 1H), 0.94 (d, J = 6.4 Hz, 3H). LC−MS (method 3a): t_R (min) = 2.23. MS (ESI+): m/z = 236 $[M + H]^+$.

2-[(3*S*,6*S*)-6-Methylmorpholin-3-yl]ethanol (73). 2-[(3*S*,6*S*)-4-Benzyl-6-methylmorpholin-3-yl]ethanol **72** (58.0 g, 246 mmol) was initially charged in ethanol (1.50 L), 10% palladium on carbon (2.90 g) and 20% palladium hydroxide on carbon (2.90 g) were added under argon atmosphere, and the mixture was then stirred under an atmosphere of hydrogen at standard pressure overnight. The reaction solution was filtered through Celite, and the filter residue was washed with hot ethanol (100 mL). The filtrate was concentrated under reduced pressure and the product was dried under high vacuum. Yield: 35.5 g (99%). ^{1}H NMR (400 MHz, chloroform-*d*): δ = 3.80−3.90 (m, 2H), 3.67−3.76 (m, 1H), 3.59−3.66 (m, 1H), 3.42−3.56 (m, 1H), 3.12 (br s, 2H), 2.89−3.00 (m, 1H), 2.75−2.87 (m, 1H), 2.61−2.73 (m, 1H), 2.23−2.41 (m, 1H), 1.45 (dd, J = 3.5, 14.6 Hz, 1H), 1.15 (d, J = 6.3 Hz, 3H). Optical rotation: 89.7° (c = 0.565, chloroform). LC−MS (method 4a): t_R (min) = 0.54. MS (ESI+): m/z = 146 $[M + H]^+$. LC−MS (method 1a): MS (ESI+): m/z = 146 $[M + H]^+$.

Methyl 2-{[(1*S*)-1-(3-Chlorophenyl)-2-fluoroethyl]amino}-7-methoxy-1,3-benzoxazole-5-carboxylate (74). Under argon atmosphere, methyl 2-chloro-7-methoxy-1,3-benzoxazole-5-carboxylate **58** (125 g, 517 mmol) was initially charged in *N*,*N*-dimethylformamide (850 mL), and (1*S*)-1-(3-chlorophenyl)-2-fluoroethanamine hydrochloride **65** (114 g, 543 mmol) and *N*,*N*-diisopropylethylamine (360 mL, 2.07 mol) were added at room temperature. The reaction solution was stirred at 70 °C (oil bath

https://dx.doi.org/10.1021/acs.jmedchem.0c01035
J. Med. Chem. XXXX, XXX, XXX−XXX

temperature) for 4 h, (1*S*)-1-(3-chlorophenyl)-2-fluoroethanamine hydrochloride **65** (8.69 g, 41.4 mmol) was then added, and the mixture was stirred at room temperature overnight (about 14 h). A further (1*S*)-1-(3-chlorophenyl)-2-fluoroethanamine hydrochloride **65** (1.09 g, 5.17 mmol) was added, and the mixture was stirred at 70 °C (oil bath temperature) for 2 h and then concentrated under reduced pressure. The residue was taken up in *tert*-butyl methyl ether (2.0 L), and the organic phase was washed with water (3 × 1.0 L). Under reduced pressure, the organic phase was concentrated to about one-third of its original volume, and the precipitated solid was then filtered off under reduced pressure. The solid precipitated in the aqueous phase was likewise filtered off under reduced pressure and then washed with *tert*-butyl methyl ether (2 × 100 mL). The combined solids were dried under high vacuum. Yield: 181 g (92%). ^{1}H NMR (400 MHz, DMSO-d_6) δ = 9.10 (d, J = 8.7 Hz, 1H), 7.59 (s, 1H), 7.36−7.52 (m, 4H), 7.31 (d, J = 1.1 Hz, 1H), 5.16−5.37 (m, 1H), 4.50−4.82 (m, 2H), 3.96 (s, 3H), 3.84 (s, 3H). Optical rotation: 77.20° (c = 0.465, methanol). LC−MS (method 4a): t_R (min) = 2.57. MS (ESI+): m/z = 379 $[M + H]^+$.

2-{[{[(1*S*)-1-(3-Chlorophenyl)-2-fluoroethyl]amino}-7-methoxy-1,3-benzoxazole-5-carboxylic Acid (75). Methyl 2-{[(1*S*)-1-(3-chlorophenyl)-2-fluoroethyl]amino}-7-methoxy-1,3-benzoxazole-5-carboxylate **74** (181 g, 478 mmol) was initially charged in 1,4-dioxane (2.4 L), and a cold (about 8 °C) solution of 45% strength aqueous sodium hydroxide solution (287 mL, 4.78 mol) in water (2.35 L) was then added. The mixture was stirred at room temperature for 4 h and then diluted with water (2.0 L). The reaction solution was extracted with *tert*-butyl methyl ether (2 × 1.0 L), ice was added to the aqueous phase, and the aqueous phase was acidified with concentrated hydrogen chloride solution (about 450 mL). The mixture was stirred at 10 °C for 15 min, the precipitated solid was filtered off under reduced pressure, and the residue was washed with water (2 × 1.0 L), left at room temperature overnight, and then dried at 60 °C for 4 h and then at 50 °C under reduced pressure until the mass remained constant. Yield: 172 g (98%, purity 89%). ^{1}H NMR (400 MHz, DMSO-d_6): δ = 12.9 (br s, 1H), 9.06 (d, J = 8.8 Hz, 1H), 7.59 (s, 1H), 7.35−7.51 (m, 4H), 7.31 (d, J = 1.3 Hz, 1H), 5.18−5.33 (m, 1H), 4.51−4.82 (m, 2H), 3.95 (s, 3H). LC−MS (method 1a): t_R (min) = 0.92. MS (ESI+): m/z = 365 $[M + H]^+$.

(2-{[(1*S*)-1-(3-Chlorophenyl)-2-fluoroethyl]amino}-7-methoxy-1,3-benzoxazol-5-yl)[(2*S*,5*S*)-5-(2-hydroxyethyl)-2-methylmorpholin-4-yl]methanone (51). 2-{[-{[(1*S*)-1-(3-Chlorophenyl)-2-fluoroethyl]amino}-7-methoxy-1,3-benzoxazole-5-carboxylic acid **75** (500 mg, 1.23 mmol, purity 89%) and 2-[(3*S*,6*S*)-6-methylmorpholin-3-yl]ethanol **73** (232 mg, 1.60 mmol) were initially charged in *N*,*N*-dimethylformamide (20.0 mL), and *N*,*N*-diisopropylethylamine (477 mg, 643 μL, 3.69 mmol) was added. Afterward, HATU (654 mg, 1.72 mmol) was added at room temperature, and the mixture was stirred for 14 h and then purified without any further workup by preparative RP-HPLC (acetonitrile/water). Traces of the minor isomer were removed by SFC on a chiral phase according to method 1d from the product obtained. Yield: 423 mg (70%). ^{1}H NMR (400 MHz, DMSO-d_6): δ = 8.98 (br s, 1H), 7.58 (s, 1H), 7.32−7.51 (m, 3H), 6.85 (br d, J = 7.21 Hz, 1H), 6.70 (br s, 1H), 5.16−5.32 (m, 1H), 4.13−4.82 (m, 4H), 3.92 (s, 3H), 3.20−3.83 (m, 10H), 2.59−3.08 (m, 1H), 1.71−2.04 (m, 2H), 0.87−1.23 (m, 3H). Optical rotation: 63.79° (c = 0.625, chloroform). HPLC (method 2e): t_R (min) = 14.0, 99.9% de. LC−MS (method 1a): t_R (min) = 0.93. MS (ESI+): m/z = 492 $[M + H]^+$.

Thrombin Crystallization and Inhibitor Complex Formation. α-Thrombin (Haemochrom Diagnostica, Germany) was dissolved in 20 mM phosphate buffer, pH 7.5, 350 mM NaCl, and 2 mM benzamidine to a final concentration of 10 mg/mL. A 4-fold excess of hirudin (Bachem) was added, and the mixture was incubated for 2 h on ice. Crystallization was performed using vapor diffusion in sitting drops, using equal volumes of protein solution and reservoir solution (0.02 M phosphate buffer, pH 7.5, 27% PEG 8000, 100 mM NaCl). Thrombin seeds were added to the final drop. Crystals with a size of ~0.2−0.4 mm grew overnight at 10 °C. All thrombin inhibitors were dissolved to give 50 mM DMSO stock solutions. DMSO stocks were diluted with reservoir solution to a final concentration of 5 mM inhibitor. Crystals of thrombin were soaked overnight in this solution at 10 °C.

Thrombin Data Collection, Processing, and Refinement. For data collection, a crystal was plunged into a solution containing 15% glycerol and was mounted at 100 K on a Rigaku 007 diffractometer equipped with a MAR image plate detector. Only **51** (BAY1217224) was mounted at 100 K on a Bruker Proteum 235 system equipped with a CCD detector. All data were processed using MOSFLM[39] and SCALA[40] from the CCP4 suite.[41] Compound **51** (BAY1217224) was processed using SAINT and SADABS from the Proteum suite (Bruker AXS). Structure solution was performed using PHASER[42] with a known in-house structure. Refinement was performed using REFMAC5.[43] The ligands were generated using PRODRG[44] and docked into the electron density within COOT.[45] Data collection and refinement statistics for all data sets are summarized in Table S5. The absolute structures were determined without any doubt in all complex X-ray structures.

PXR Expression, Purification, and Cocrystallization. An expression construct identical to the one reported by Wang et al.,[46] coding for a peptide of the nuclear receptor coactivator NCOA1 (residues 678−700) fused via a GGSGG linker to the C-terminus of the ligand binding domain of the PXR (residues 129−434), was expressed in *E. coli*, purified via affinity chromatography (HisTrap, 5 mL), ion-exchange chromatography (Mono S HR 10/10), and gel filtration [Superdex 75 26/60, 20 mM Tris buffer, pH 7.8, 250 mM NaCl, 2.5 mM EDTA, 5% (v/v) glycerol, 5 mM DTT], concentrated to 12.1 mg/mL, and shock-frozen in liquid nitrogen. For cocrystallization with compound **17**, the PXR was thawed, supplemented with 25 mM compound (from a 500 mM stock solution in DMSO), and incubated at 277 K for 24 h. Crystals were formed using the vapor diffusion method in hanging drops consisting of 1 μL of protein−ligand solution and 1 μL of reservoir solution [100 mM imidazole, pH 8.0, 20% (v/v) MPD (2-methyl-2,4-pentanediol)].

PXR Data Collection, Processing, and Refinement. For data collection, crystals were briefly immersed in cryo buffer [100 mM imidazole, pH 8.0, 30% (v/v) MPD] and shock-frozen in liquid nitrogen. A diffraction data set to 1.85 Å resolution was collected on beamline BL14.1 operated by the Helmholtz-Zentrum Berlin (HZB) at the BESSY II electron storage ring (Berlin-Adlershof, Germany)[47] and processed using XDS[48] via the graphical user interface XDSAPP.[49] The structure was solved by rigid body refinement with REFMAC5[43] with PDB entry 3HVL as starting model. The initial model was rebuilt in COOT[45] and refined using REFMAC5. Difference electron density indicated binding of the ligand only in one of the two PXR molecules in this crystal form (chain B). The ligand parameters were calculated using PRODRG,[44] and the ligand was fitted to the electron density using COOT. The final ligand occupancy was adjusted to 0.70. Density in the ligand binding pocket of chain A was modeled as MPD (artifact from the crystallization reservoir solution) which may also be present as a minor component in chain B (here not modeled). Data collection and refinement statistics are summarized in Table S5.

PXR Transactivation Assay. To evaluate PXR nuclear receptor transactivation, a screening luciferase reporter gene assay in human HepG2 cells was applied. HepG2 cells were seeded in a 384-well plate and cultivated at 37 °C in humidified air with 5% CO_2. 48 h prior to readout, cells were transiently co-transfected with a vector for human PXR and a luciferase reporter gene under the control of the human CYP3A4 promotor with FuGENE HD transfection reagent (Promega, Madison, WI, USA) according to the manufacturer's instructions. 24 h after seeding, the cells were treated with test compound (2 nM to 50 μM, 0.5% DMSO) prepared by a 1:3 serial dilution. Rifampicin was incubated in the same manner, as a positive control. In addition, for normalization of the luminescence signal, cells were incubated with rifampicin at a concentration of 50 or 16.7 μM corresponding to 100% activation, as well as with DMSO for background luminescence corresponding to 0% activation (n = 32 wells each). After treatment, cells were lysed and incubated with the luciferase substrate ONE-Glo reagent (Promega, Madison, WI, USA) according to the manufac-

https://dx.doi.org/10.1021/acs.jmedchem.0c01035
J. Med. Chem. XXXX, XXX, XXX−XXX

turer's instructions, and the luminescence signal was detected using a plate reader. The assay was validated with a standard set of inducers (e.g., bosentan, carbamazepine) and noninducers (e.g., penicillin V, fluconazole). From the dose−response curves, a concentration-dependent increase in the luciferase activity above 4-fold standard deviation of the DMSO background was classified as PXR transactivation and is represented as the minimum efficacious concentration (MEC).

Human Hepatocyte Assay for CYP3A4 Induction. Human hepatocytes were seeded at a density of ∼40 000 cells/96 wells in a collagen sandwich and cultured for 1 d before compound treatment. Cells were treated with a 1:3 serial dilution of eight concentrations for 2 consecutive days with media change every day. After compound treatment for 48 h, cells were lysed and mRNA was prepared by a state-of-the-art magnetic beads technique. In brief, approximately 24 h after the last treatment, hepatocytes were harvested for mRNA isolation. Thus, cell culture medium was removed from each well, cells were washed with 150 μL of supplement-free cell culture medium prior to cell lysis, cells were lysed with 100 μL of lysis buffer containing proteinase K (50 μg/μL, final concentration in well: 30 ng/μL), and final cell lysates were stored at −80 °C. mRNA was isolated using the Dynabeads mRNA Direct Kit (Life Technologies, Germany). 150 μL of each cell lysate was mixed with 100 μg magnetic beads and incubated for a few minutes; then, the supernatant was removed and the beads were washed twice with washing buffer A and twice with washing buffer B with 200 and 100 μL per well, respectively. Single-stranded cDNA was prepared from mRNA with the high capacity RNA-to-cDNA kit (Life Technologies). 20 μL RT Master Mix [comprised of 10× RT buffer, 25× deoxyNTPs, 10× Random Hexamers, RNase inhibitor (20 U/μL), MultiScribe reverse transcriptase (50 U/μL), and RNase-free water] was added to each well and transcribed for 60 min at 37 °C using the Gene Amp PCR System 9700 thermocycling program (Biometra, Göttingen, Germany). The prepared cDNA samples were stored at −80 °C prior to analysis by quantitative RT-PCR, which was carried out on a QuantStudio7 Flex PCR system (Applied Biosystems) according to the manufacturer's protocol. A primer mix was prepared for each gene expression assay. A typical primer mix contained TaqMan Fast Advanced Master Mix (1×), gene expression assay (1×, 900 nM forward and reverse primers), and RNase-free water and was added to the cDNA. The relative quantity of the target cDNA compared to that of the control cDNA (actin, tubulin) was determined by the ΔΔCt method. Relative quantification measures the change in mRNA expression in a test sample relative to that in a control sample (e.g., vehicle treated). CYP induction was calculated based on the ΔΔCt method and expressed as fold induction over the vehicle-treated control.

***In Vitro* Clearance Determinations with Rat Hepatocytes.** Incubations with rat hepatocytes (freshly prepared from male Whistar rats) were performed at 37 °C, pH 7.4, in a total volume of 1.5 mL using a modified Janus robotic system (PerkinElmer). The incubation mixtures contained 1×10^6 cells/mL (corrected, according to viability of the cells, determined via microscopy after staining with trypan blue), 1 μM substrate, and Williams' medium E (Sigma, product no. W1878). The final acetonitrile concentration was <1%. Aliquots of 125 μL were withdrawn from the incubation mixture after 2, 10, 20, 30, 50, 70, and 90 min and dispensed in a 96-well plate containing acetonitrile (250 μL) to stop the reaction. After centrifugation, supernatants were analyzed by LC−MS/MS (AB Sciex Triple Quad 5500). The calculation of *in vitro* clearance values from half-life data using rat hepatocytes, reflecting substrate depletion, was performed using the following equation: $CL'_{intrinsic}$ [mL/(min·kg)] = (0.693/*in vitro* $t_{1/2}$ [min])·(liver weight [g liver/kg body mass])·(cell no. [1.1×10^8]/liver weight [g])/(cell no. [1×10^6]/incubation volume [mL]). The CL_{blood} was estimated using the nonrestricted well-stirred model: CL_{blood} well-stirred [L/(h·kg)] = (Q_H [L/(h·kg)]·$CL'_{intrinsic}$ [L/(h·kg)])/(Q_H [L/(h·kg)] + $CL'_{intrinsic}$ [L/(h·kg)]). For calculations, the following values were used: rat specific liver weight of 32 g/kg body mass, hepatic blood flow of 4.2 L/(h·kg); the cell number in the liver was estimated to be 1.1×10^8 cells/g liver.

Caco-2 Permeability Assay. Caco-2 cells (DSMZ, German Resource Centre for Biological Material, Braunschweig, Germany) were seeded at a density of 4×10^4 cells/well on 24-well polycarbonate insert plates, 0.4 μm pore size (Corning Life Sciences, Lowell, MA), and maintained for 15 d in Dulbecco's modified Eagle medium supplemented with 10% fetal BSA, 20 mM glucose, 10 mg/500 mL streptomycin, and 10000 IU/500 mL penicillin in a humidified incubator at 8% CO_2. Before the assay was run, the culture medium was replaced by transport buffer consisting of Hanks' balanced salt solution (pH 7.4) supplemented with 10 mM HEPES and 20 mM glucose. Stock solutions of test compounds were prepared in DMSO and diluted 100-fold with transport buffer. These solutions were applied to either the apical or the basolateral compartment, and 1% DMSO was added to the buffer in the trans-compartment. After an incubation of 2 h at 37 °C, samples were taken from both compartments and analyzed by LCMS/MS. Transepithelial electrical resistance (TEER) was measured in Hanks' balanced salt solution before and after the transport studies using an STX 100 TEER electrode (World Precision Instruments, Berlin, Germany). To ensure the integrity of the cell monolayer, TEER values were determined before and after an experiment. The acceptance criterion for acceptable batches of cell monolayers was a TEER value of 600 Ω. P_{app} was calculated as $(V_r/P_0)\cdot(1/S)\cdot(P_2/t)$, where V_r is the volume of medium in the receiver chamber, P_0 is the measured peak height or peak area of the test drug in the donor chamber at t_0, S is the surface area of the monolayer, P_2 is the measured peak height or peak area of the test drug in the acceptor chamber after an incubation of 2 h, and t is the incubation time (2 h). The efflux ratio was calculated as $P_{app}(B-A)/P_{app}(A-B)$, where $P_{app}(B-A)$ and $P_{app}(A-B)$ represent the apparent permeability of test compound from the basolateral to apical and apical to basolateral side of the cellular monolayer, respectively. Cell data are expressed as arithmetic means and SD. The SD for the efflux ratio was calculated using linear error propagation.

***In Vivo* Pharmacokinetics in Rats.** Animal studies were conducted in accordance with the German Animal Protection Act (Deutsches Tierschutzgesetz). For the determination of pharmacokinetic parameters, male Wistar rats strain Hannover (Harlan Winkelmann, Borchen, Germany) were catheterized under isoflurane (Delta Select, Dreieich, Germany) anesthesia. One day after implantation of the catheter, compounds were administered either intravenously by direct injection into the lateral tail vein at doses of 0.3 to 0.5 mg/kg, 2 mL/kg in plasma containing 2% DMSO, or orally at a dose of 1 mg/kg, 5 mL/kg (10% ethanol/40% PEG/50% demineralized water, v/v/v) by gavage using a calibrated glass syringe. Blood samples were collected at 0.033, 0.083, 0.25, 0.5, 1, 2, 3, 5, 7, and 24 h postdosing for iv and 0.083, 0.25, 0.5, 1, 2, 3, 5, 7, and 24 h postdosing for po, via the catheter. After centrifugation, plasma was precipitated by the addition of acetonitrile.

The supernatants were subjected to HPLC performed on an Agilent 1200 liquid chromatography system (Agilent Technologies, Waldbronn, Germany). The mobile phase consisted of 10 mM ammonium acetate (pH 3.0) and acetonitrile, and a linear gradient from 20% to 90% acetonitrile (v/v) within 2 min was applied. Tandem mass spectrometry was performed on an API 3000, 4000, or 5500 triple quadrupole mass spectrometer (Applied Biosystems, Darmstadt, Germany) connected to the HPLC system through a TurboIonSpray interface. Pharmacokinetic parameters were calculated from plasma concentrations with Kinex, a validated in-house (Bayer AG, Wuppertal, Germany) calculation program.

In all sets of experiments, blood samples were collected in heparinized syringes following exsanguination by a cut through the carotid artery under deep isoflurane anesthesia (approximately 2.5% v/v). Blood cells were separated from plasma by centrifugation, and the plasma was stored for further analyses.

Biochemical Assays for Determination of Thrombin Inhibition and Selectivity against Other Serine Proteases. Inhibitory potency and/or selectivity of test compounds were determined. The assays are based on the fluorescent detection of aminomethylcoumarine (AMC), released from the fluorogenic peptidic protease substrates upon protease catalyzed cleavage.

https://dx.doi.org/10.1021/acs.jmedchem.0c01035
J. Med. Chem. XXXX, XXX, XXX−XXX

The active proteases or zymogenes, typically purified from human plasma, and corresponding substrates are commercially available. All enzymes and substrates are diluted in assay buffer (50 mM Tris/HCl, pH 7.4, 100 mM NaCl, 5 mM $CaCl_2$, 0.1% BSA).

Serine protease assays comprise of the following enzymes and substrates. The final assay concentrations are given: thrombin (Kordia; 0.02 nM), Boc-Asp(OBzl)-Pro-Arg-AMC (Bachem I-1560; 5 μM); factor Xa (Kordia; 1.3 nM), Boc-Ile-Glu-Gly-Arg-AMC (Bachem I-1100; 5 μM); factor XIa (Kordia; 0.15 nM), Boc-Glu(OBzl)-Ala-Arg-AMC (Bachem I-1575; 5 μM); plasmin (Kordia; 0.1 μg/mL, 1.2 nM), MeOSuc-Ala-Phe-Lys-AMC (Bachem I-1275; 50 μM); tissue plasminogen activator (tPA, Loxo; 2 nM), CH_3SO_2-D-Phe-Gly-Arg-AMC (Pentapharm 091-06; 5 μM); Kallikrein (Kordia; 0.2 nM), H-Pro-Phe-Arg-AMC (Bachem I-1295; 5 μM); trypsin (Sigma; 2.5 ng/mL, 0.1 nM), substrate Boc-Ile-Glu-Gly-Arg-AMC (Bachem I-1100; 5 μM)

Coupled protease reactions are applied for assaying factor VIIa: factor VIIa (Kordia; 0.5 pM), tissue factor (1:1000 RecombiPlasTin2G, Bedford, USA), factor X (Kordia; 0.07 U/mL, 12 nM), factor Xa substrate Boc-Ile-Glu-Gly-Arg-AMC (Bachem I-1100; 50 μM); factor X is premixed with factor Xa substrate.

For determination of test compound potency, the enzyme and corresponding substrate dilutions are used to perform protease assays. To 384 well microtiter plates (white, Greiner), containing 1 μL/well serial dilutions of test or reference compounds, 20 μL of assay buffer, 20 μL of enzyme dilution, and 20 μL of substrate (mix) are added. Control reactions do not contain test compound (DMSO only). After incubation for typically 30 min (linear reaction kinetics) at room temperature, fluorescence (ex 360 nm, em 465 nm) is measured in a microtiter plate fluorescence reader (e.g., Tecan Safire II). IC_{50} values are determined by plotting log test compound concentration against the percentage protease activity.

Determination of the Anticoagulatory Activity. The anticoagulatory activity of test substances was determined *in vitro* in human plasma, rabbit plasma, and rat plasma. Blood was drawn off in a mixing ratio of sodium citrate/blood of 1:9 using 0.11 M sodium citrate solution as receiver. Immediately thereafter, the blood was mixed thoroughly and centrifuged at ~4000*g* for 15 min to separate the plasma.

The prothrombin time (PT, synonyms: thromboplastin time, quick test) was determined in the presence of various concentrations of test substance using a commercial test kit [Neoplastin (Boehringer, Mannheim, Germany) or Hemoliance RecombiPlasTin (Instrumentation Laboratory, Lexington, MA)]. Test compounds were incubated with the plasma at 37 °C for 3 min. Coagulation was then started by the addition of thromboplastin, and the time when coagulation occurred was determined. The concentration of test substance which led to a doubling of the PT is reported as the EC_{200}.

Arteriovenous Shunt and Hemorrhage Model (Combimodel Rat). Animal studies were conducted in accordance with the German Animal Protection Act (Deutsches Tierschutzgesetz). Fasting male rats (strain: HsdCpd:WU) with a weight of 300−350 g were anesthetized using Inactin (150−180 mg/kg). Thrombus formation was initiated in an arteriovenous shunt in accordance with the method described by Christopher N. Berry;[50] thus, the left jugular vein and the right carotid artery were exposed and connected by an extracorporeal shunt, using a polyethylene tube (PE 60) with a length of 10 cm. In the middle, this polyethylene tube was attached to a further polyethylene tube (PE 160) with a length of 3 cm which contained a roughened nylon thread arranged to form a loop, to provide a thrombogenic surface. Compound **51** was administered at three dose levels as iv bolus with subsequent continuous iv infusion to exclude the impact of pharmacokinetic differences on the *in vivo* assessment. 20 min after the iv bolus administration of **51**, the extracorporeal circulation was opened for 15 min. Subsequently, the shunt was removed and the thrombus on the nylon thread was weighed.

To determine the bleeding time, immediately after opening of the shunt circulation, the tip of the tail of the rat was cut by 3 mm using a razor blade. The tail was placed into physiological saline kept at 37 °C, and the bleeding from the cut was observed for 15 min. The time until the bleeding ceased for at least 30 s was determined.

Rat Venous Stasis Model. Thrombus formation was induced in anesthetized rats (n = 6−10 per dose group) as described previously, with minor modifications. The abdominal vena cava was exposed, and two loose sutures (8−10 mm apart) were placed below the left renal venous branch. Compound **51** dissolved in PEG/water/glycerol (996 g/100 g/60 g), or vehicle, was given by oral gavage (po) administration 90 min before thrombus induction. Thromboplastin (0.5 mg/kg) was injected into a femoral vein, and after 15 s, the proximal and distal sutures were tied; 15 min later, the ligated segment was removed, and the thrombus was withdrawn and weighed.

■ ASSOCIATED CONTENT

Supporting Information

The Supporting Information is available free of charge at https://pubs.acs.org/doi/10.1021/acs.jmedchem.0c01035.

(A) Synthesis of compounds **10**, **13**−**19**, **20a**/**20b**, **21**−**26**, **27a**/**27b**, **28**−**32**, **33a**/**33b**, **34**−**36**, **37a**/**37b**, **38**−**41**, **42a**/**42b**, **43**−**50**, and **52**; (B) ^{1}H NMR data of intermediates **53**−**58**, **60**−**62**, **64**−**65**, **67**−**69**, **72**−**75**, and BAY1217224 (**51**); (C) Tables S1−S4 (PDF)

Molecular formula strings and some data (XLSX)

Accession Codes

The coordinates and structure factors have been deposited to the Protein Data Bank (PDB) with the following accession codes for thrombin cocomplex structures: 6ZUG (compound **10**), 6ZUH (compound **17**), 6ZUN (compound **20a**), 6ZUU (compound **31**), 6ZUW (compound **40**), 6ZV8 (compound **51**), 6ZUX (compound **42a**), 6ZV7 (compound **42b**), and 6TFI (PXR cocrystal structure with cmpd **17**). Authors will release the atomic coordinates upon article publication.

■ AUTHOR INFORMATION

Corresponding Author

Alexander Hillisch − *Research and Development, Bayer AG, Pharmaceuticals, 42103 Wuppertal, Germany*; orcid.org/0000-0002-4228-2347; Email: alexander.hillisch@bayer.com

Authors

Kersten M. Gericke − *Research and Development, Bayer AG, Pharmaceuticals, 42103 Wuppertal, Germany*

Swen Allerheiligen − *Research and Development, Bayer AG, Pharmaceuticals, 42103 Wuppertal, Germany*

Susanne Roehrig − *Research and Development, Bayer AG, Pharmaceuticals, 42103 Wuppertal, Germany*

Martina Schaefer − *Research and Development, Bayer AG, Pharmaceuticals, 13342 Berlin, Germany*

Adrian Tersteegen − *Research and Development, Bayer AG, Pharmaceuticals, 42103 Wuppertal, Germany*

Simone Schulz − *Research and Development, Bayer AG, Pharmaceuticals, 42103 Wuppertal, Germany*

Philip Lienau − *Research and Development, Bayer AG, Pharmaceuticals, 13342 Berlin, Germany*

Mark Gnoth − *Research and Development, Bayer AG, Pharmaceuticals, 42103 Wuppertal, Germany*

Vera Puetter − *Research and Development, Bayer AG, Pharmaceuticals, 13342 Berlin, Germany*

Roman C. Hillig − *Research and Development, Bayer AG, Pharmaceuticals, 13342 Berlin, Germany*

Stefan Heitmeier − *Research and Development, Bayer AG, Pharmaceuticals, 42103 Wuppertal, Germany*

Complete contact information is available at:

https://pubs.acs.org/10.1021/acs.jmedchem.0c01035

Notes

The authors declare the following competing financial interest(s): All authors are employed at Bayer AG or a subsidiary of Bayer AG.

■ ACKNOWLEDGMENTS

We thank Petra Rothhaupt and Ivonne Herms for excellent technical support with PXR purification and crystallization and the staff of beamline BL14.1 at the Helmholtz-Zentrum Berlin (HZB) for excellent support during data collection. We thank Kay Greenfield for critical review of the manuscript.

■ ABBREVIATIONS USED

FVIIa, factor VIIa; FIXa, factor IXa; FXa, factor Xa; FXIa, factor XIa; Caco-2, colon carcinoma cell line; EBP, ester binding pocket; MEC, minimum efficacious concentration; OAH, oxyanion hole; S1, S2, S3, S4 pockets, substrate binding pockets of proteinases; P1, P2, P3, P4, substrate residues of proteinases; LLE, lipophilic ligand efficiency; CYP3A4, cytochrome P450 3A4; HATU, *O*-(7-azabenzotriazol-1-yl)-*N*,*N*,*N*′,*N*′-tetramethyluronium hexafluorophosphate

■ REFERENCES

(1) Eriksson, U. G.; Bredberg, U.; Hoffmann, K. J.; Thuresson, A.; Gabrielsson, M.; Ericsson, H.; Ahnoff, M.; Gislen, K.; Fager, G.; Gustafsson, D. Absorption, distribution, metabolism, and excretion of ximelagatran, an oral direct thrombin inhibitor, in rats, dogs, and humans. *Drug Metab. Dispos.* **2003**, *31*, 294−305.

(2) Hauel, N. H.; Nar, H.; Priepke, H.; Ries, U.; Stassen, J. M.; Wienen, W. Structure-based design of novel potent nonpeptide thrombin inhibitors. *J. Med. Chem.* **2002**, *45*, 1757−1766.

(3) Straub, A.; Roehrig, S.; Hillisch, A. Oral, direct thrombin and factor Xa inhibitors: the replacement for warfarin, leeches, and pig intestines? *Angew. Chem., Int. Ed.* **2011**, *50*, 4574−4590.

(4) Roehrig, S.; Straub, A.; Pohlmann, J.; Lampe, T.; Pernerstorfer, J.; Schlemmer, K. H.; Reinemer, P.; Perzborn, E. Discovery of the novel antithrombotic agent 5-chloro-N-({(5S)-2-oxo-3- [4-(3-oxo-morpholin-4-yl)phenyl]-1,3-oxazolidin-5-yl}methyl)thiophene- 2-carboxamide (BAY 59-7939): an oral, direct factor Xa inhibitor. *J. Med. Chem.* **2005**, *48*, 5900−5908.

(5) Wong, P. C.; Pinto, D. J.; Zhang, D. Preclinical discovery of apixaban, a direct and orally bioavailable factor Xa inhibitor. *J. Thromb. Thrombolysis* **2011**, *31*, 478−492.

(6) Chan, L.; Pisano, M. Edoxaban (Savaysa): A factor Xa inhibitor. *P T* **2015**, *40*, 651−695.

(7) Zhang, P.; Huang, W.; Wang, L.; Bao, L.; Jia, Z. J.; Bauer, S. M.; Goldman, E. A.; Probst, G. D.; Song, Y.; Su, T.; Fan, J.; Wu, Y.; Li, W.; Woolfrey, J.; Sinha, U.; Wong, P. W.; Edwards, S. T.; Arfsten, A. E.; Clizbe, L. A.; Kanter, J.; Pandey, A.; Park, G.; Hutchaleelaha, A.; Lambing, J. L.; Hollenbach, S. J.; Scarborough, R. M.; Zhu, B. Y. Discovery of betrixaban (PRT054021), N-(5-chloropyridin-2-yl)-2-(4-(N,N-dimethylcarbamimidoyl)benzamido)-5-methoxybenz amide, a highly potent, selective, and orally efficacious factor Xa inhibitor. *Bioorg. Med. Chem. Lett.* **2009**, *19*, 2179−2185.

(8) Burgey, C. S.; Robinson, K. A.; Lyle, T. A.; Nantermet, P. G.; Selnick, H. G.; Isaacs, R. C.; Lewis, S. D.; Lucas, B. J.; Krueger, J. A.; Singh, R.; Miller-Stein, C.; White, R. B.; Wong, B.; Lyle, E. A.; Stranieri, M. T.; Cook, J. J.; McMasters, D. R.; Pellicore, J. M.; Pal, S.; Wallace, A. A.; Clayton, F. C.; Bohn, D.; Welsh, D. C.; Lynch, J. J., Jr.; Yan, Y.; Chen, Z.; Kuo, L.; Gardell, S. J.; Shafer, J. A.; Vacca, J. P. Pharmacokinetic optimization of 3-amino-6-chloropyrazinone acetamide thrombin inhibitors. Implementation of P3 pyridine N-oxides to deliver an orally bioavailable series containing P1 N-benzylamides. *Bioorg. Med. Chem. Lett.* **2003**, *13*, 1353−1357.

(9) Chobanian, H. R.; Pio, B.; Guo, Y.; Shen, H.; Huffman, M. A.; Madeira, M.; Salituro, G.; Terebetski, J. L.; Ormes, J.; Jochnowitz, N.; Hoos, L.; Zhou, Y.; Lewis, D.; Hawes, B.; Mitnaul, L.; O'Neill, K.; Ellsworth, K.; Wang, L.; Biftu, T.; Duffy, J. L. Improved stability of proline-derived direct thrombin inhibitors through hydroxyl to heterocycle replacement. *ACS Med. Chem. Lett.* **2015**, *6*, 553−557.

(10) Abrahamsson, K.; Andersson, P.; Bergman, J.; Bredberg, U.; Brånalt, J.; Egnell, A.-C.; Eriksson, U.; Gustafsson, D.; Hoffman, K.-J.; Nielsen, S.; Nilsson, I.; Pehrsson, S.; Polla, M. O.; Skjaeret, T.; Strimfors, M.; Wern, C.; Ölwegård-Halvarsson, M.; Örtengren, Y. Discovery of AZD8165 − a clinical candidate from a novel series of neutral thrombin inhibitors. *MedChemComm* **2016**, *7*, 272−281.

(11) Allerheiligen, S.; Bauser, M.; Schirok, H.; Haerter, M.; Siegel, S.; Rester, U.; Gerdes, C.; Heitmeier, S.; von Degenfeld, G.; Buchmueller, A.; Dittrich-Wengenroth, E.; Saatmann, U.; Strassburger, J.; Gnoth, J. M.; Lang, D. Oxazolidinones. WO2008155069, 2008.

(12) Bauser, M.; Buchmueller, A.; Bruens, A.; von Degenfeld, G.; Dittrich-Wengenroth, E.; Gerdes, C.; Gnoth, M.; Gnoth, J.; Gottschling, D.; Heitmeier, S.; Hendrix, M.; Koebberling, J.; Lang, D.; Rester, U.; Saatmann, U.; Schneider, D.; Siegel, S.; Strassburger, J.; Wilmen, A.; Tersteegen, A. Acylaminoimidazoles. WO2007082666, 2007.

(13) Bauser, M.; Buchmueller, A.; von Degenfeld, G.; Dittrich-Wengenroth, E.; Gerdes, C.; Gnoth, M.; Gnoth, J.; Gottschling, D.; Heitmeier, S.; Hendrix, M.; Koebberling, J.; Lang, D.; Rester, U.; Saatmann, U.; Tersteegen, A.; Bruens, A. Acyl Aminoimidazoles and Acyl Aminothiazoles. WO2008043533 2007.

(14) Bauser, M.; Buchmueller, A.; von Degenfeld, G.; Dittrich-Wengenroth, E.; Gerdes, C.; Gnoth, M.; Gnoth, J.; Gottschling, D.; Heitmeier, S.; Hendrix, M.; Koebberling, J.; Lang, D.; Rester, U.; Saatmann, U.; Tersteegen, A.; Bruens, A. Acylaminopyrazoles. WO2008046527, 2008.

(15) Schneider, D.; Buchmueller, A.; Dittrich-Wengenroth, E.; Gerdes, C.; Gnoth, M.; Gnoth, J.; Heitmeier, S.; Hendrix, M.; Rester, U.; Saatmann, U.; Siegel, S. Benzoxazoles. WO2007140982, 2007.

(16) Siegel, S.; Schneider, D.; Buchmueller, A.; Dittrich-Wengenroth, E.; Gerdes, C.; Gnoth, M.; Gnoth, J.; Heitmeier, S.; Hendrix, M.; Rester, U.; Saatmann, U. 2-(Heteroaryl) Alkyl Indazole 6-phenyl and Thienyl Methyl Amide. WO2008006479, 2008.

(17) Cheng, A. C.; Coleman, R. G.; Smyth, K. T.; Cao, Q.; Soulard, P.; Caffrey, D. R.; Salzberg, A. C.; Huang, E. S. Structure-based maximal affinity model predicts small-molecule druggability. *Nat. Biotechnol.* **2007**, *25*, 71−75.

(18) Halgren, T. A. Identifying and characterizing binding sites and assessing druggability. *J. Chem. Inf. Model.* **2009**, *49*, 377−389.

(19) Leo, A. Calculating logPoct from structures. *Chem. Rev.* **1993**, *93*, 1281.

(20) Ertl, P.; Rohde, B.; Selzer, P. Fast calculation of molecular polar surface area as a sum of fragment-based contributions and its application to the prediction of drug transport properties. *J. Med. Chem.* **2000**, *43*, 3714−3717.

(21) Lobell, M.; Hendrix, M.; Hinzen, B.; Keldenich, J.; Meier, H.; Schmeck, C.; Schohe-Loop, R.; Wunberg, T.; Hillisch, A. In silico ADMET traffic lights as a tool for the prioritization of HTS hits. *ChemMedChem* **2006**, *1*, 1229−1236.

(22) Abel, R.; Young, T.; Farid, R.; Berne, B. J.; Friesner, R. A. Role of the active-site solvent in the thermodynamics of factor Xa ligand binding. *J. Am. Chem. Soc.* **2008**, *130*, 2817−2831.

(23) Young, T.; Abel, R.; Kim, B.; Berne, B. J.; Friesner, R. A. Motifs for molecular recognition exploiting hydrophobic enclosure in protein-ligand binding. *Proc. Natl. Acad. Sci. U. S. A.* **2007**, *104*, 808−813.

(24) Lazaridis, T. Inhomogeneous fluid approach to solvation thermodynamics. I. Theory. *J. Phys. Chem. B* **1998**, *102*, 3531−3541.

(25) Jorgensen, W. L.; Maxwell, D. S.; Tirado-Rives, J. Development and testing of the OPLS all-atom force field on conformational energetics and properties of organic liquids. *J. Am. Chem. Soc.* **1996**, *118*, 11225−11236.

(26) Ryckmans, T.; Edwards, M. P.; Horne, V. A.; Correia, A. M.; Owen, D. R.; Thompson, L. R.; Tran, I.; Tutt, M. F.; Young, T. Rapid assessment of a novel series of selective CB(2) agonists using parallel synthesis protocols: A Lipophilic Efficiency (LipE) analysis. *Bioorg. Med. Chem. Lett.* **2009**, *19*, 4406−4409.
(27) Hopkins, A. L.; Groom, C. R.; Alex, A. Ligand efficiency: a useful metric for lead selection. *Drug Discovery Today* **2004**, *9*, 430−431.
(28) Friesner, R. A.; Banks, J. L.; Murphy, R. B.; Halgren, T. A.; Klicic, J. J.; Mainz, D. T.; Repasky, M. P.; Knoll, E. H.; Shelley, M.; Perry, J. K.; Shaw, D. E.; Francis, P.; Shenkin, P. S. Glide: a new approach for rapid, accurate docking and scoring. 1. Method and assessment of docking accuracy. *J. Med. Chem.* **2004**, *47*, 1739−1749.
(29) Nagata, T.; Yoshino, T.; Haginoya, N.; Yoshikawa, K.; Isobe, Y.; Furugohri, T.; Kanno, H. Cycloalkanediamine derivatives as novel blood coagulation factor Xa inhibitors. *Bioorg. Med. Chem. Lett.* **2007**, *17*, 4683−4688.
(30) Sastry, G. M.; Adzhigirey, M.; Day, T.; Annabhimoju, R.; Sherman, W. Protein and ligand preparation: parameters, protocols, and influence on virtual screening enrichments. *J. Comput.-Aided Mol. Des.* **2013**, *27*, 221−234.
(31) Sherman, W.; Day, T.; Jacobson, M. P.; Friesner, R. A.; Farid, R. Novel procedure for modeling ligand/receptor induced fit effects. *J. Med. Chem.* **2006**, *49*, 534−553.
(32) Allerheiligen, S.; Buchmüller, A.; Engel, K.; Gerdes, C.; Gericke, K. M.; Gerisch, M.; Heitmeier, S.; Hillisch, A.; Kinzel, T.; Lienau, P.; Riedl, B.; Röhrig, S.; Schmidt, M. V.; Strassburger, J.; Tersteegen, A. Substituted Benzoxazoles. WO2014195231 2013.
(33) Allerheiligen, S.; Buchmüller, A.; Engel, K.; Gerdes, C.; Gericke, K. M.; Gerisch, M.; Heitmeier, S.; Hillisch, A.; Kinzel, T.; Lienau, P.; Riedl, B.; Röhrig, S.; Schmidt, M. V.; Strassburger, J.; Tersteegen, A. Triazolopyridines as Thrombin Inhibitors for the Treatment of Thromboembolic Diseases. WO2014195244, 2013.
(34) Allerheiligen, S.; Buchmüller, A.; Engel, K.; Gerdes, C.; Gericke, K. M.; Gerisch, M.; Heitmeier, S.; Hillisch, A.; Kinzel, T.; Lienau, P.; Riedl, B.; Röhrig, S.; Schmidt, M. V.; Strassburger, J. Substituted Benzoxazoles. WO2014195230, 2013.
(35) Cho, S. H.; Kim, J. Y.; Lee, S. Y.; Chang, S. Silver-mediated direct amination of benzoxazoles: tuning the amino group source from formamides to parent amines. *Angew. Chem., Int. Ed.* **2009**, *48*, 9127−9130.
(36) Lok, R.; Leone, R. E.; Williams, A. J. Facile rearrangements of alkynylamino heterocycles with noble metal cations. *J. Org. Chem.* **1996**, *61*, 3289−3297.
(37) Chen, Z.; Zhu, W.; Zheng, Z.; Zou, X. One-pot α-nucleophilic fluorination of acetophenones in a deep eutectic solvent. *J. Fluorine Chem.* **2010**, *131*, 340−344.
(38) Thvedt, T. H. K.; Fuglseth, E.; Sundby, E.; Hoff, B. H. Microwave assisted fluorination: an improved method for side chain fluorination of substituted 1-arylethanones. *Tetrahedron* **2009**, *65*, 9550−9556.
(39) Battye, T. G.; Kontogiannis, L.; Johnson, O.; Powell, H. R.; Leslie, A. G. iMOSFLM: a new graphical interface for diffraction-image processing with MOSFLM. *Acta Crystallogr., Sect. D: Biol. Crystallogr.* **2011**, *67*, 271−281.
(40) Evans, P. R. Scaling and assessment of data quality. *Acta Crystallogr., Sect. D: Biol. Crystallogr.* **2006**, *D62*, 72−82.
(41) Winn, M. D.; Ballard, C. C.; Cowtan, K. D.; Dodson, E. J.; Emsley, P.; Evans, P. R.; Keegan, R. M.; Krissinel, E. B.; Leslie, A. G.; McCoy, A.; McNicholas, S. J.; Murshudov, G. N.; Pannu, N. S.; Potterton, E. A.; Powell, H. R.; Read, R. J.; Vagin, A.; Wilson, K. S. Overview of the CCP4 suite and current developments. *Acta Crystallogr., Sect. D: Biol. Crystallogr.* **2011**, *67*, 235−242.
(42) Read, R. J. Pushing the boundaries of molecular replacement with maximum likelihood. *Acta Crystallogr., Sect. D: Biol. Crystallogr.* **2001**, *57*, 1373−1382.
(43) Winn, M. D.; Murshudov, G. N.; Papiz, M. Z. Macromolecular TLS refinement in REFMAC at moderate resolutions. *Methods Enzymol.* **2003**, *374*, 300−321.
(44) Schüttelkopf, A. W.; van Aalten, D. M. PRODRG: a tool for high-throughput crystallography of protein-ligand complexes. *Acta Crystallogr., Sect. D: Biol. Crystallogr.* **2004**, *60*, 1355−1363.
(45) Emsley, P.; Lohkamp, B.; Scott, W. G.; Cowtan, K. Features and development of Coot. *Acta Crystallogr., Sect. D: Biol. Crystallogr.* **2010**, *66*, 486−501.
(46) Wang, W.; Prosise, W. W.; Chen, J.; Taremi, S. S.; Le, H. V.; Madison, V.; Cui, X.; Thomas, A.; Cheng, K. C.; Lesburg, C. A. Construction and characterization of a fully active PXR/SRC-1 tethered protein with increased stability. *Protein Eng., Des. Sel.* **2008**, *21*, 425−433.
(47) Mueller, U.; Darowski, N.; Fuchs, M. R.; Forster, R.; Hellmig, M.; Paithankar, K. S.; Puhringer, S.; Steffien, M.; Zocher, G.; Weiss, M. S. Facilities for macromolecular crystallography at the Helmholtz-Zentrum Berlin. *J. Synchrotron Radiat.* **2012**, *19*, 442−449.
(48) Kabsch, W. Xds. *Acta Crystallogr., Sect. D: Biol. Crystallogr.* **2010**, *66*, 125−132.
(49) Sparta, K. M.; Krug, M.; Heinemann, U.; Müller, U.; Weiss, M. S. XDSAPP2.0. *J. Appl. Crystallogr.* **2016**, *49*, 1085−1092.
(50) Berry, C. N.; Girard, D.; Lochot, S.; Lecoffre, C. Antithrombotic actions of argatroban in rat models of venous, 'mixed' and arterial thrombosis, and its effects on the tail transection bleeding time. *Br. J. Pharmacol.* **1994**, *113*, 1209−1214.

https://dx.doi.org/10.1021/acs.jmedchem.0c01035
J. Med. Chem. XXXX, XXX, XXX−XXX